doi: 10.4208/cicp.300112.100812a

Development and Application of a Reduced Order Model for the Control of Self-Sustained Instabilities in Cavity Flows

Kaushik Kumar Nagarajan[1,*], Laurent Cordier[2] and Christophe Airiau[3]

[1] *National Aerospace Laboratories, Bengaluru, 560017, India.*
[2] *PPRIME Institute CEAT, 43 route de l'aérodrome, 86000 Poitiers, France.*
[3] *Université de Toulouse; INPT, UPS; IMFT (Institut de Mécanique des Fluides de Toulouse); Allée Camille Soula, F-31400 Toulouse, France.*

Abstract. Flow around a cavity is characterized by a self-sustained mechanism in which the shear layer impinges on the downstream edge of the cavity resulting in a feedback mechanism. Direct Numerical Simulations of the flow at low Reynolds number has been carried out to get pressure and velocity fluctuations, for the case of un-actuated and multi frequency actuation. A Reduced Order Model for the isentropic compressible equations based on the method of Proper Orthogonal Decomposition has been constructed. The model has been extended to include the effect of control. The Reduced Order dynamical system shows a divergence in time integration. A method of calibration based on the minimization of a linear functional of error, to the sensitivity of the modes, is proposed. The calibrated low order model is used to design a feedback control of cavity flows based on an observer design. For the experimental implementation of the controller, a state estimate based on the observed pressure measurements is obtained through a linear stochastic estimation. Finally the obtained control is introduced into the Direct Numerical Simulation to obtain a decrease in spectra of the cavity acoustic mode.

AMS subject classifications: 93C05, 93C10, 76N25

Key words: Reduced order modelling, proper orthogonal decomposition, cavity flows, feedback control.

1 Introduction

Self sustained instabilities in compressible cavities arise due to the impingement of the shear layer on the downstream edge of the cavity, and is caused by the energetic coherent

*Corresponding author. *Email addresses:* kaushik@ctfd.cmmacs.ernet.in (K. K. Nagarajan), laurent.cordier@univ-poitiers.fr (L. Cordier), Christophe.Airiau@imft.fr (C. Airiau)

structure, resulting in a pressure feedback mechanism which induces the far field noise in the cavity. The flow is characterized by a strong coupling between the hydrodynamic instability and the acoustic propagation which can be sometimes intense. Applications of such flows arise in airframe fuel vents, landing gears, weapon bays. Accurate modelling of the cavity noise is important from the point of view of a search for quieter aircrafts. The traditional tools for the modelling of the cavity like Direct Numerical Simulation (DNS) and Large Eddy Simulation (LES) pose difficulties in terms of computational resources, also the constraint increases when the ultimate aim of study is in the application of control. The self sustained instabilities in cavity has been studied in the past by many authors [1–5]. The principles of Reduced Order Modelling (ROM) based on Proper Orthogonal Decomposition (POD) and a Galerkin projection, has been in the past applied to model and control to flows with self-sustained instabilities, like wake behind cylinder [6] and high lift configurations [7]. Flow past an open cavity has already been studied using ROM by [8] and [9] but without any application to flow control. More recently, ROM for controlled configurations has been proposed by [10,11]. In [12] the ROM for flows issued from an experiment has been used to design a controller. The major hurdle in using the ROM for control applications is the accuracy of the model in predicting the dynamics of the system even for short periods, also difficulty arises when the control parameters are changed as in a real time simulation. Various numerical strategies termed as calibration techniques has been developed in the recent past based on the solution of an optimization problem and can be found in the works of [6,13–16]. A summary of the application of various method has been discussed in detail [17] where a method of calibration based on the Tikhonov regularization has been proposed. The main contribution of this paper is then to complete the full development as applied to cavities, like building up the ROM, including the effect of control, calibrating the model and finally performing control studies. We give further developments to the calibration technique by performing a sensitivity analysis to weight the importance of the errors in the different modes of the ROM, and accurately predict the dynamics of the system. The ROM thus obtained has been applied to perform the feedback control of cavity flows to obtain a reduction in the noise level of the cavity.

The paper is organized as follows. In Section 2 the derivation of the plant model used for control studies has been discussed. The general principles of model reduction is discussed in Subsection 2.1 where the usual ROM based on the principle of Galerkin projection is obtained as a special case. In Subsection 2.2 we discuss the general principles POD, followed by a discussion of the ROM for the isentropic equations in Subsection 2.2.1. Extension of ROM to include the effect of actuation is presented in Subsection 2.3. Section 3 concerns the calibration of the ROM to accurately represent the temporal dynamics, the various errors that define the dynamics of the ROM are presented in Subsection 3.1. A new approach to Tikhonov based regularization based on the sensitivity analysis is presented in Subsection 3.2 to obtain an accurate representation of the dynamics. The ROM has been applied to the cavity flow configuration in Section 4. Finally feedback control law based on the estimation of the observer dynamics has been presented in Section 5.

2 Derivation of the plant model

2.1 Model reduction principles

To present the general ideas consider a physical system of the form

$$\mathcal{S}: \begin{cases} \dot{\boldsymbol{a}}(t) = \boldsymbol{f}(t, \boldsymbol{a}(t), \gamma(t)), \\ \boldsymbol{b}(t) = \boldsymbol{g}(t, \boldsymbol{a}(t), \gamma(t)). \end{cases} \tag{2.1}$$

The RHS can be considered as any evolutionary model representing the dynamics, for example the Navier-Stokes equations. Although the ideas are easily extended to infinite dimension we present them for a finite dimensional case which is justified considering the usual approach of numerically resolving the equations by discretization in n space dimension. $\boldsymbol{a} \in \mathbb{R}^n$ represents the state variables, $\gamma \in \mathbb{R}^m$ represents the inputs or the control applied to the flow, and $\boldsymbol{b} \in \mathbb{R}^p$ represents the output of observables. The RHS of (2.1) can be linearized to obtain a state-space form as

$$\mathcal{S}_{LTI}: \begin{cases} E\ \dot{\boldsymbol{a}}(t) = A\boldsymbol{a}(t) + B\gamma(t), \\ \boldsymbol{b}(t) = C\boldsymbol{a}(t) + D\gamma(t), \end{cases} \tag{2.2}$$

where $E \in \mathbb{R}^{n\times n}$, $A \in \mathbb{R}^{n\times n}$, $B \in \mathbb{R}^{n\times m}$, $C \in \mathbb{R}^{p\times n}$ and $D \in \mathbb{R}^{p\times m}$. E need not necessarily be invertible. The dimension of the model usually corresponds to the dimension of the spatial discretization which can be very large, hence the principle of model reduction seeks a subspace V of dimension $r \ll n$. The non-linear reduced order model corresponding to (2.1) can be written as

$$\widehat{\mathcal{S}}: \begin{cases} \dot{\hat{\boldsymbol{a}}}(t) = \hat{\boldsymbol{f}}(t, \hat{\boldsymbol{a}}(t), \gamma(t)), & \hat{\boldsymbol{a}} \in \mathbb{R}^r, \\ \hat{\boldsymbol{b}}(t) = \hat{\boldsymbol{g}}(t, \hat{\boldsymbol{a}}(t), \gamma(t)), & \hat{\boldsymbol{b}} \in \mathbb{R}^p, \end{cases} \quad \text{with} \quad r \ll n, \tag{2.3}$$

and the corresponding linear reduced model as

$$\widehat{\mathcal{S}}_{LTI}: \begin{cases} \hat{E}\ \dot{\hat{\boldsymbol{a}}}(t) = \hat{A}\ \hat{\boldsymbol{a}}(t) + \hat{B}\ \gamma(t), \\ \hat{\boldsymbol{b}}(t) = \hat{C}\ \hat{\boldsymbol{a}}(t) + \hat{D}\ \gamma(t). \end{cases} \tag{2.4}$$

The reduced subspace has to have the following desirable properties when used as an approximation to the high fidelity model (2.1):

1. $\|b - \hat{b}\| < \epsilon \times \|\gamma\| \quad \forall \gamma$ where ϵ is the tolerance.
2. The model need to preserve the stability of the attractor, and be passive, *i.e.* entropy conserving approximation to the high fidelity model $\mathcal{S}$.
3. Must be efficient to reproduce the most important features of the high fidelity model.

To present the idea of projection, from now on we just consider the linear model $\widehat{\mathcal{S}}$. We seek biorthogonal matrices V and W of size $\mathbb{R}^{n\times r}$ such that $W^TQV = I_r$ where $Q \in \mathbb{R}^{n\times n}$ is a weight matrix. The Reduced Order Model is obtained by a projection of the state variable a on the matrix V such that $\boldsymbol{a} = V\ \hat{\boldsymbol{a}}$ and $\hat{\boldsymbol{y}} \simeq \boldsymbol{y}$. One defines the residue $\boldsymbol{\mathcal{R}}$ to measure the accuracy of the projection, $\boldsymbol{a} \simeq V\hat{\boldsymbol{a}}$ as

$$\boldsymbol{\mathcal{R}} = EV\ \dot{\hat{\boldsymbol{a}}}(t) - AV\hat{\boldsymbol{a}}(t) - B\gamma(t), \tag{2.5a}$$

$$\hat{\boldsymbol{b}}(t) = CV\ \hat{\boldsymbol{a}}(t) + D\gamma(t). \tag{2.5b}$$

The Petrov-Galerkin projection is obtained by requiring the residue orthogonal to the approximated space, *i.e.* $W^TQ\boldsymbol{\mathcal{R}} = \mathbf{0}_r$. The projection matrices of the system $\hat{\mathcal{S}}_{LTI}$ can now be obtained after a simple calculation as

$$\hat{A} = W^TQAV, \qquad \hat{B} = W^TQB, \qquad \hat{C} = CV,$$
$$\hat{D} = D, \qquad \hat{E} = W^TQEV.$$

The well known Galerkin projection is obtained by taking $V \equiv W$. Several projection methods exist for the linear system (2.2). Examples are the Krylov subspace method for the controllability matrix which relies on the identification of the moments of transfer function [18], projection on the dominant modes of controllability and observability matrix [19, 20], projection of global stability modes [21], POD based projection method on the subspace determined from the snapshots [22] in which the flow fields are decomposed into energy ranked coherent structures. This is the method used in this work and is briefly described in the next section.

2.2 Proper orthogonal decomposition

The basic idea of a POD is to decompose the flow field into energy ranked coherent structures represented by mathematical modes the details of which can be found in [23, 24]. Let H denote any Hilbert space with an inner product denoted by $(\cdot,\cdot)$ and the norm induced by the inner product denoted by $\|\cdot\|$. In the fluid dynamic context the space H consist of functions defined on some spatial domain Ω on which the fluid evolves, usually $H = L^2(\Omega)$. Let $\boldsymbol{q}(\boldsymbol{x},t)$ be any vector of flow variable, where $\boldsymbol{x}$ and $t \in [0,T]$ denote respectively the spatial variables and the time of the numerical simulation or experimental measurements. We also assume a discrete sampling of our data in time and space. We seek an expansion for $\boldsymbol{q}$ of the form

$$\boldsymbol{q}(\boldsymbol{x},t) = \overline{\boldsymbol{q}}(\boldsymbol{x}) + \sum_{i=1}^{n} a_i(t)\boldsymbol{\phi_i}(\boldsymbol{x}), \tag{2.6}$$

where $\overline{\boldsymbol{q}}$ denotes the average of the n flow snapshots. The spatial modes $\boldsymbol{\phi_i}(\boldsymbol{x})$ and the temporal coefficients $a_i(t)$ are determined by solving an eigenvalue problem involving the time correlation tensor that minimizes the average projection error:

$$E(\|\boldsymbol{q} - P_S\boldsymbol{q}\|). \tag{2.7}$$

E denotes the averaging operator, for instance the ensemble average ($E = \frac{1}{n}\sum_{i=1}^{n}$) and P_S denote the projection operator over the space $S \subset H$ and dimension m. Note that the problem of minimizing $E(\|\boldsymbol{q} - P_S\boldsymbol{q}\|)$ is equivalent to maximizing $E(\|P_S\boldsymbol{q}\|^2)$, the "energy" of the orthogonal projection since by Pythogoraus theorem we have $\|\boldsymbol{q}\|^2 = \|\boldsymbol{q} - P_S\boldsymbol{q}\|^2 + \|P\boldsymbol{q}\|^2$. Solving the optimization problem leads to an eigenvalue problem for the spatial modes $\boldsymbol{\phi}$ given by

$$R\boldsymbol{\phi} = \lambda\boldsymbol{\phi}, \tag{2.8}$$

where $R : H \to H$ is the linear operator defined as

$$R = E(\boldsymbol{q}_k \otimes \boldsymbol{q}_k^*). \tag{2.9}$$

Here $\boldsymbol{q}^* \in H^*$ denotes the dual of $\boldsymbol{q}$, given by $\boldsymbol{q}^*(\cdot) = (\cdot, \boldsymbol{q})$ and $\otimes$ is the usual tensor product[†]. One can easily verify that R is self adjoint *i.e.* $(R\,x, y) = (x, R\,y)$ and hence by the spectral theorem the eigenfunctions $\boldsymbol{\phi}$ can be chosen to be orthonormal, The eigenvalues λ are then determined by taking the inner product of Eq. (2.8) with $\boldsymbol{\phi}$ to obtain

$$\lambda = E\left(|(\boldsymbol{q}_k, \boldsymbol{\phi})|^2\right). \tag{2.10}$$

The eigenvalues λ in the above equation represents the average energy in the projection of the ensemble onto $\boldsymbol{\phi}$ where energy is defined in sense of the induced norm. We also conclude that the R is positive semi-definite, and the eigenfunctions $\boldsymbol{\phi}_j$ which maximize $E(\|P_S\boldsymbol{q}_k\|^2)$ are the eigenfunctions corresponding to the largest eigenvalues. Also the eigenfunctions reproduce almost every member of the ensemble (except on a set of measure zero). One can also verify that the range of the operator R is contained in the span of the ensemble $\boldsymbol{q}_k$ and that any eigenfunction $\boldsymbol{\phi}$ can be written as linear combination of snapshots:

$$\boldsymbol{\phi} = \sum_{k=1}^{n} c_k \boldsymbol{q}_k, \tag{2.11}$$

where the coefficients $c_k \in \mathbb{R}$. If the average operator E over the snapshots $\boldsymbol{q}_k$ is given as

$$E(f(\boldsymbol{q})) = \sum_{k=1}^{n} \alpha_k f(\boldsymbol{q}_k), \tag{2.12}$$

where $\alpha_k > 0$ satisfies $\sum_{k=1}^{n} \alpha_k = 1$ (usually giving equally weights to snapshots *i.e.* $\alpha_k = 1/m$). The eigenvalue problem (2.8) may be written in terms of the coefficients c_k as

$$R\,c = \lambda c, \tag{2.13}$$

where $c = (c_1, \cdots, c_m)$ and R is an $m \times m$ correlation matrix with $R_{ij} = \alpha_i\left(\boldsymbol{q}_j, \boldsymbol{q}_i\right)$. This is the usual method of snapshots as described [22]. Here we note that the direct problem involves solving an eigenvalue problem possibly on an infinite dimensional space H which

[†]We have $(\boldsymbol{u} \otimes \boldsymbol{v}^*)(\boldsymbol{\psi}) = \boldsymbol{u}(\boldsymbol{\psi}, \boldsymbol{v})$, $\forall \boldsymbol{u}, \boldsymbol{v}, \boldsymbol{\psi} \in H$.

may be very large, on the other hand the method of snapshots involve solving only an m dimensional eigenvalue problem and the method proves computationally efficient if m is small compared with the dimension of H. Having described the POD procedure we now proceed to build a ROM as explained in the next section.

2.2.1 ROM for cavity flows

The Reduced Order Model is obtained by performing a Galerkin projection of the governing dynamics (for instance the Navier-Stokes equations) onto the spatial modes determined from the POD procedure. Two ROM models for cavities has been proposed in [9], one using the full compressible equations and the other with an isentropic approximation. In this work we use the isentropic equations for compressible flows [8], which is a valid physical models for flows at moderate Mach number. Scaling the stream-wise and span-wise component of velocities u,v by the free stream velocity U_∞, the local sound speed c by the ambient sound speed c_∞, the lengths by the cavity depth D (see Fig. 2), and time by D/U_∞, the equations are given by

$$\begin{aligned}
&u_t+uu_x+vu_y+\frac{1}{M^2}\frac{2}{\gamma-1}cc_x=\frac{1}{Re}(u_{xx}+u_{yy}),\\
&v_t+uv_x+vv_y+\frac{1}{M^2}\frac{2}{\gamma-1}cc_y=\frac{1}{Re}(v_{xx}+v_{yy}),\\
&c_t+uc_x+vc_y+\frac{\gamma-1}{2}c(u_x+v_y)=0,
\end{aligned}$$

where $M=U_\infty/a_\infty$ is the Mach number and $Re=U_\infty D/\nu$ is the Reynolds number. If we denote $\boldsymbol{q}=(u,v,c)$ the vector of flow variables, the above equations can be recasted as

$$\dot{\boldsymbol{q}}=\frac{1}{Re}\boldsymbol{L}(\boldsymbol{q})+\frac{1}{M^2}\boldsymbol{Q_1}(\boldsymbol{q},\boldsymbol{q})+\boldsymbol{Q_2}(\boldsymbol{q},\boldsymbol{q}), \tag{2.14}$$

with

$$\boldsymbol{L}(\boldsymbol{q})=\begin{bmatrix}u_{xx}+u_{yy}\\ v_{xx}+v_{yy}\\ 0\end{bmatrix},\quad \boldsymbol{Q_1}(\boldsymbol{q^1},\boldsymbol{q^2})=-\frac{2}{\gamma-1}\begin{bmatrix}c^1c^2_x\\ c^1c^2_y\\ 0\end{bmatrix},\quad \boldsymbol{Q_2}(\boldsymbol{q^1},\boldsymbol{q^2})=-\begin{bmatrix}u^1u^2_x+v^1u^2_y\\ u^1v^2_x+v^1v^2_y\\ u^1c^2_x+v^1c^2_y\\ +\frac{\gamma-1}{2}c^1(u^2_x+v^2_y)\end{bmatrix}.$$

To obtain the reduced order model by means of a Galerkin projection we define an inner product on the state space as

$$(\boldsymbol{q_1},\boldsymbol{q_2})_\Omega=\int_\Omega\left(u_1u_2+v_1v_2+\frac{2\alpha}{\gamma-1}c_1c_2\right)d\Omega,$$

where α is a constant and γ is the ratio of specific heats. In this work we choose the value of $\alpha=1$, which gives the definition of stagnation enthalpy while calculating the norm.

The above definition ensures the stability of the origin of the attractor as demonstrated by [8]. We use expansion (2.6) and the definition of the inner product given above to perform the Galerkin projection of the isentropic equations onto the first $n \ll N_{POD}$ spatial eigenfunctions, to obtain the Reduced Order Model as

$$\begin{aligned}
\dot{a}_i^R(t) &= \frac{1}{Re}C_i^1 + \frac{1}{M^2}C_i^2 + C_i^3 + \sum_{j=1}^{n}\left(\frac{1}{Re}L_{ij}^1 + \frac{1}{M^2}L_{ij}^2 + L_{ij}^3\right)a_j^R(t) \\
&\quad + \sum_{j,k=1}^{n}\left(\frac{1}{M^2}Q_{ijk}^1 + Q_{ijk}^2\right)a_j^R(t)a_k^R(t) \\
&= C_i + \sum_{j=1}^{n}L_{ij}a_j^R(t) + \sum_{j,k=1}^{n}Q_{ijk}a_j^R(t)a_k^R(t) \\
&= f_i(\underbrace{C_i, \boldsymbol{L_i}, \boldsymbol{Q_i}}_{\boldsymbol{y}}, \boldsymbol{a}^R(t)) = \boldsymbol{f}(\boldsymbol{y}, \boldsymbol{a}^R(t)),
\end{aligned} \tag{2.15}$$

where f_i is a polynomial of degree 2 in $\boldsymbol{a}^R$ and the coefficients of the projection are given by

$$\begin{aligned}
&C_i^1 = (\boldsymbol{\phi_i}, \boldsymbol{L}(\overline{\boldsymbol{q}}))_\Omega, && L_{ij}^1 = \left(\boldsymbol{\phi_i}, \boldsymbol{L}(\boldsymbol{\phi_j})\right)_\Omega, && Q_{ijk}^1 = \left(\boldsymbol{\phi_i}, \boldsymbol{Q_1}(\boldsymbol{\phi_j}, \boldsymbol{\phi_k})\right)_\Omega, \\
&C_i^2 = (\boldsymbol{\phi_i}, \boldsymbol{Q_1}(\overline{\boldsymbol{q}}, \overline{\boldsymbol{q}}))_\Omega, && L_{ij}^2 = \left(\boldsymbol{\phi_i}, \boldsymbol{Q_1}(\overline{\boldsymbol{q}}, \boldsymbol{\phi_j}) + \boldsymbol{Q_1}(\boldsymbol{\phi_j}, \overline{\boldsymbol{q}})\right)_\Omega, && Q_{ijk}^2 = \left(\boldsymbol{\phi_i}, \boldsymbol{Q_2}(\boldsymbol{\phi_j}, \boldsymbol{\phi_k})\right)_\Omega, \\
&C_i^3 = (\boldsymbol{\phi_i}, \boldsymbol{Q_2}(\overline{\boldsymbol{q}}, \overline{\boldsymbol{q}}))_\Omega, && L_{ij}^3 = \left(\boldsymbol{\phi_i}, \boldsymbol{Q_2}(\overline{\boldsymbol{q}}, \boldsymbol{\phi_j}) + \boldsymbol{Q_2}(\boldsymbol{\phi_j}, \overline{\boldsymbol{q}})\right)_\Omega.
\end{aligned}$$

2.3 ROM for the actuated flow

Having discussed the ROM for the un-actuated case we now move on to introduce the effect of actuation. The advantage of the reduced order models can be fully exploited when they are capable of being used in control studies. We would also like to have a dynamical system where the actuation effect is naturally embedded. There has been recent attempts to take care of the introduction of actuation in [10,25] for a feedback control where snapshots from the controlled case are augmented with the un-actuated modes (baseline flow as it is usually called) to obtain a global representation for the controlled case. The regions where the control is introduced is explicitly identified while performing the projections, hence are termed as input separation methods. To explain further the flow domain Ω into two sub-regions, such that $\Omega = \Omega_{ac} + \Omega_{unac}$ where Ω_{ac}, Ω_{unac} represents the actuated and the un-actuated part of the domain respectively. The inner product for the corresponding domains is defined as $(\cdot,\cdot) = (\cdot,\cdot)_{\Omega_{ac}} + (\cdot,\cdot)_{\Omega_{unac}}$, with the corresponding boundary condition imposed for Ω_{ac}. This procedure yields an autonomous system of ODE's of the form, on using the summation convention as.

$$\dot{a}_k = C_k + L_{ik}a_k + Q_{ijk}a_i a_j + h_{1k}\gamma + h_{2ik}a_i\gamma + h_{3k}\gamma^2, \tag{2.16}$$

where γ is the actuation signal. Another procedure of introducing the actuation in the ROM is to identify the system coefficients of the actuated model based on a stochastic

estimation technique, to give a ROM of the form (2.16) as in [25]. The main disadvantages of the above methods is that they are quite cumbersome, as one has to explicitly identify the region of separation where the actuation is introduced, where there is a possibility of mismatch with the base line modes. Also the information of the input actuation is hidden in the model. One then looks for an alternative separation method to include the effect of actuation on the base line model as discussed in [11], *i.e.* one seeks an expansion of the form

$$\mathbf{q}(\mathbf{x},t) = \overline{\mathbf{q}}(\mathbf{x}) + \sum_{i=1}^{n} a_i(t)\boldsymbol{\phi_i}(\mathbf{x}) + \gamma(t)\boldsymbol{\psi}(\mathbf{x}), \tag{2.17}$$

where γ is the actuation and $\boldsymbol{\psi}$ is the spatial actuated coefficient and which should ideally satisfy the following conditions:

1. The actuation effect should be explicitly available in our ROM and should be able to reproduce the un-actuated dynamics in case the value of actuation tends to zero.

2. Most of the actuated dynamics are well captured by the un-actuated POD modes and hence the completion of the full actuated dynamics is obtained by an extension of the bases of the un-actuated case. This condition is an additional constraint to condition 1 in that we require a constraint on the dimension of our actuation, by specifying that the base-line modes capture most of the dynamics. This is the crux of the whole problem.

3. We further strengthen the above condition by imposing an optimality condition by requiring that the energy not captured by (2.17) is minimal.

Fig. 1 summaries the above condition. The conditions above leads to the following algorithm due to [11].

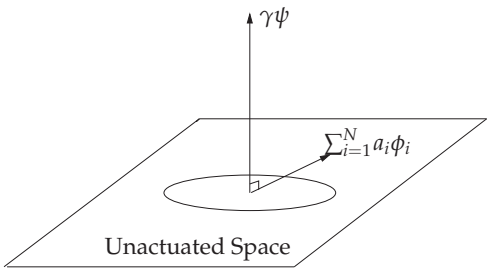

Figure 1: Schematic representation of the actuated expansion, the actuated mode is orthogonal to the unactuated space.

Algorithm 2.1

1. To start with, let the actuated snapshot sets be denoted as $\left\{\mathbf{q_k^{ac}}, \gamma_k\right\}_{k=1}^{m}$, where $\gamma_k = \gamma(t_k)$ is the value of the actuation, $\mathbf{q_k^{ac}} = \mathbf{q^{ac}}(\mathbf{x}, t_k)$ and m is the number of actuated snapshots.

2. We subtract the mean $\overline{\mathbf{q}}$ of the un-actuated base flow from the snapshot set. We define a new set of realizations by an innovation operator given as

$$\tilde{\mathbf{q}}_{\mathbf{k}} = \mathbf{q}_k^{ac} - P_{\mathcal{S}}\mathbf{q}_k^{ac} = \mathbf{q}_k^{ac} - \sum_{i=1}^{n} (\mathbf{q}_k^{ac}, \boldsymbol{\phi_i})_{\Omega} \boldsymbol{\phi_i}$$

to care of the part of the actuated mode which can be captured well by the un-actuated subspace.

3. We then wish to construct an orthogonal subspace to the un-actuated space to capture the effect of actuation. This is done by solving an L_2 minimization problem for the functional given by

$$\mathcal{J}(\boldsymbol{\psi}) = E\left[\|\tilde{\mathbf{q}}_{\mathbf{k}} - \gamma_k \boldsymbol{\psi}\|^2\right],$$

where E is any averaging operator.

4. The solution of the above minimization problem is given by

$$\boldsymbol{\psi} = \frac{E[\gamma_k \tilde{\mathbf{q}}_{\mathbf{k}}]}{E[\gamma_k^2]}.$$

5. The expansion for the flow field can now be written for the actuated case as

$$\mathbf{q}^{ac}(\mathbf{x},t) = \overline{\mathbf{q}}^{\mathbf{ac}}(\mathbf{x}) + \sum_{i=1}^{n} a_i^{ac}(t)\boldsymbol{\phi_i}(\mathbf{x}) + \gamma(t)\boldsymbol{\psi}(\mathbf{x}).$$

With this expansion the Galerkin projection of (2.14) gives

$$\begin{aligned} \dot{a}_i^{ac}(t) = C_i + \sum_{j=1}^{n} L_{ij} a_j^{ac}(t) + \sum_{j,k=1}^{n} Q_{ijk} a_j^{ac}(t) a_k^{ac}(t) + h_{1i}\gamma(t) \\ + \sum_{j=1}^{n} h_{2ij} a_j^{ac}(t)\gamma(t) + h_{3i}\gamma^2(t), \end{aligned} \tag{2.18}$$

where

$$\begin{aligned} h_{1i} &= \frac{1}{Re}(\boldsymbol{\phi_i}, \boldsymbol{L}(\boldsymbol{\psi}))_{\Omega} + (\boldsymbol{\phi_i}, \boldsymbol{Q}(\overline{\boldsymbol{q}}, \boldsymbol{\psi}))_{\Omega} + (\boldsymbol{\phi_i}, \boldsymbol{Q}(\boldsymbol{\psi}, \overline{\boldsymbol{q}}))_{\Omega}, \\ h_{2ij} &= \left(\boldsymbol{\phi_i}, \boldsymbol{Q}(\boldsymbol{\phi_j}, \boldsymbol{\psi})\right)_{\Omega} + \left(\boldsymbol{\phi_i}, \boldsymbol{Q}(\boldsymbol{\psi}, \boldsymbol{\phi_j})\right)_{\Omega}, \qquad h_{3i} = (\boldsymbol{\phi_i}, \boldsymbol{Q}(\boldsymbol{\psi}, \boldsymbol{\psi}))_{\Omega}, \end{aligned}$$

with $\boldsymbol{Q}(\cdot,\cdot) = \frac{1}{M^2}\boldsymbol{Q_1}(\cdot,\cdot) + \boldsymbol{Q_2}(\cdot,\cdot)$.

To study the effect of actuation on the unactuated baseline modes we observe from (2.18) the actuated temporal modes are given by

$$a_i^{ac}(t) = (\boldsymbol{\phi_i}, \boldsymbol{q}^{ac} - \overline{\boldsymbol{q}}^{\boldsymbol{ac}} - \gamma(t)\boldsymbol{\psi})_{\Omega}.$$

Here we make the assumption that the average of the mean flow in un-actuated and actuated cases are equal ($\overline{\boldsymbol{q}}^{\boldsymbol{ac}} = \overline{\boldsymbol{q}}$), since the value of actuation introduced is small. The term $\boldsymbol{q}^{\boldsymbol{ac}} - \overline{\boldsymbol{q}}^{\boldsymbol{ac}}$ can now be interpreted as a translation of the reduced order subspace. On

noting this and the fact that the actuated mode is orthogonal to the un-actuated subspace *i.e.* $\boldsymbol{\psi} \perp \boldsymbol{\phi}$ the term $a_i^{ac}(t) \longrightarrow 0$. This fact is important in that while calibrating the ROM, it is sufficient to just calibrate the un-actuated parts, as will be explained in the next section. Another point worth mentioning is that the time derivative of control vanishes due to the orthogonal property of the actuated modes. We also introduce, an error to take care of the difference in the average values while performing the Galerkin projections as

$$\varepsilon_i = \frac{(\delta\overline{\boldsymbol{q}}^{ac}, \boldsymbol{\phi}_i)}{(\boldsymbol{\phi}_i, \overline{\boldsymbol{q}}^{ac})}. \tag{2.19}$$

3 Calibration of the ROM

The reduced order model (2.18) has an intrinsic problem of converging to the wrong attractor when used to simulate the flow for long time periods. Hence there is a need to identify the coefficients of the dynamical system so as to minimis the error between the actual time coefficients $a_i^P(t)$ from the POD and that obtained from the ROM $a_i^R(t)$ using a suitable norm for the error. The reasons for the inaccurate behavior of the ROM can be attributed to the truncation of the POD bases where the dissipative scales of the higher POD modes are neglected. An analogous problem occurs in the Large Eddy Simulation (LES) of flows when there is lack of dissipation due to the smaller scales. Even including all the modes in Galerkin projection may still lead to the wrong attractor due to structural instability as has been demonstrated in [26]. Other problems may arise due to the contribution of pressure at the boundaries of the domain, which is usually neglected [27]. The stability properties of the compressible POD-Galerkin approximation has been studied by [28].

3.1 Definition of errors

Three definitions of error have been defined in [17]. The natural choice is in defining $\boldsymbol{e}^1(\boldsymbol{f},t) = \boldsymbol{a}^P(t) - \boldsymbol{a}^R(t)$ but this leads to a nonlinear constrained problem (see Section 3.1.1). The other two choices being state calibration error $\boldsymbol{e}^2$ without the dynamical constraint given by

$$\mathbf{e}^2(\mathbf{y},t) = \mathbf{a}^P(t) - \mathbf{a}^P(0) - \int_0^T \mathbf{f}(\mathbf{y}, \mathbf{a}^P(\tau))d\tau$$

and the flow calibration $\boldsymbol{e}^3(\boldsymbol{f},t) = \dot{\boldsymbol{a}}^P(t) - \boldsymbol{f}(\boldsymbol{a}^P(t))$ where $\boldsymbol{f}$ is characterized by the coefficients of (2.15).

3.1.1 Nonlinear constrained problem

In this method we have to find the coefficients of the dynamical system such that the error $\boldsymbol{e}^1$ is minimized under the constraints that the coefficients $C_i, \boldsymbol{L}_i, \boldsymbol{Q}_i$ $(i = 1, \cdots, n)$ satisfy

(2.15). We rather seek to minimize $\mathcal{I}^1(\boldsymbol{f}) = \langle \|\boldsymbol{e}^1(\boldsymbol{f},t)\|^2_\Lambda \rangle_T$ where $\langle\cdot\rangle_T$ is a time averaging operator over $[0,T]$, for N_t equally spaced elements on $[0,T]$ we have

$$\langle f(t)\rangle_T = \frac{1}{N_t}\sum_{i=1}^{N_t} f(t_i), \qquad \text{with} \quad t_i = (i-1)\Delta t \quad \text{and} \quad \Delta t = \frac{T}{N_t - 1},$$

$\|.\|_\Lambda$ is a norm on $\mathbb{R}^N$. For any positive definite matrix $\Lambda \in \mathbb{R}^{N\times N}$ the norm of any vector $\mathbf{e} \in \mathbb{R}^N$ is given by

$$\|\mathbf{e}\|^2_\Lambda = \mathbf{e}^T \Lambda \mathbf{e}.$$

The matrix Λ acts as a weight function giving importance to the specific POD modes, when $\Lambda = I_N$ it means that all the POD modes have the same importance in terms of the error. This leads us to a constrained optimization problem as in [6], in which we solve backward in time, an adjoint equation given by

$$\begin{aligned}\dot{\xi}_i(t) &= -\sum_{j=1}^{n} L_{ji}\xi_j(t) - \sum_{j,k=1}^{n} \xi_j(t)(Q_{jik}+Q_{jki})a_i^R(t) - \underbrace{2\left(a_i^R(t) - a_i^P(t)\right)}_{s} \\ &= g_i(\underbrace{C_i, \boldsymbol{L_i}, \boldsymbol{Q_i}}_{\boldsymbol{y}}, \boldsymbol{a}^R(t), \boldsymbol{\xi}^R(t)) + s \;=\; \mathbf{g}(\mathbf{y}, \mathbf{a}^R, \boldsymbol{\xi}^R(t)) + s, \end{aligned} \tag{3.1}$$

where ξ_i is the adjoint variable and s the source term. The terminal condition of the above equation is given by $\xi_i(T) = 0$. The gradients of the cost functional $\mathcal{I}^{(1)}$ with respect to the coefficients C_i and $\boldsymbol{L_i}$ of the ROM are

$$\nabla\mathcal{I}^1{}_{C_i} = \int_0^T \xi_i(t)\,dt, \qquad \nabla\mathcal{I}^1{}_{\boldsymbol{L_i}} = \int_0^T \xi_i(t) a_j^R(t)\,dt$$

and represent the sensitivity of the functional to the coefficients. The corresponding optimality system (state equations, adjoint equations, optimality conditions) is solved by a gradient based method to obtain the coefficients of the reduced order model.

3.2 A weighted approach to Tikhonov regularization

In this section we introduce a new method of calibration. As demonstrated in [14] minimization of $\mathcal{I}^3(\boldsymbol{f}) = \langle \|\boldsymbol{e}^3(\boldsymbol{f},t)\|^2 \rangle_T$ leads to the solution of a linear system for the coefficients $\mathbf{y}$ defining $\boldsymbol{f}$. Unfortunately, this linear system is not well conditioned and lead to numerical divergence when the calibrated coefficients are used to integrate in time (2.15). For that purpose, [14] have introduced a new cost functional defined as a weighted sum of a term measuring the normalized error between the behavior of the model (2.15) with $\boldsymbol{f}$ and with the coefficients determined directly by Galerkin projection $\boldsymbol{f}^{GP}$ and another term linked to the distance between $\boldsymbol{f}$ and $\boldsymbol{f}^{GP}$. The value of the weighting factor which

represents the cost of calibration was chosen rather arbitrarily and hence was user dependent. In [17], a Tikhonov regularization method was suggested to improve the conditioning of the linear system. The idea of this method is to seek a regularized solution $\mathbf{y}_\rho$ as the minimizer of the following weighted functional

$$\Phi_\rho(\mathbf{y}) = \|A\mathbf{y}-\mathbf{b}\|_2^2+\rho\|\mathcal{L}(\mathbf{y}-\mathbf{y_0})\|_2^2,$$

where the first term corresponds to the residual norm, and the second to a side constraint imposed on the solution. $\mathcal{L}$ represents the discrete approximation matrix of a differential operator of order d and $\mathbf{y_0}$ a reference solution. The value ρ is chosen so as to compromise between the minimization of the norm of the residual for the linear system and the seminorm of the solution. Here, the regularization parameter ρ is determined by the classical L-curve method, as described in [17]. We have the error defined for the minimization of the functional $\mathcal{I}^i$ as

$$\mathcal{I}^i(\mathbf{y}) = \left\langle \|\mathbf{e}^i(\mathbf{y},t)\|_\Lambda^2 \right\rangle_T.$$

Usually the matrix Λ is chosen as Identity, which means that we give equal weights to all the modes in the definition of calibration. However this matrix can be chosen in suitable way so as to include the effect of mode selection in the definition. Two ways of defining the weights can be proposed:

1. We consider that the main interest is in modelling the effect of the energetic structures and hence the eigen-spectra themselves serve as a measure of the relative importance of the modes, which is the most natural choice of the weights for the definition of error.

2. The error can be based on an overall sensitivity of the model with respect to a cost functional.

The weight matrix Λ for the definition of error for the first case can be simply written as a diagonal matrix:

$$\Lambda_{ii} = \frac{\sigma_i}{\max \sigma_i} \qquad \text{for} \quad i=\{1,\cdots,N\},$$

where σ is the singular value obtained as a solution of the eigenvalue problem of the time correlation matrix. For the second case consider the state equations

$$\dot{\mathbf{a}}^R = \mathbf{f}(\mathbf{y},\mathbf{a}^R). \tag{3.2}$$

Variation of any convex cost functional $\mathcal{J}$ with respect to the state variables $\mathbf{a}^R = \{a_i^R\}_{i=1}^N$ gives the adjoint equation of (3.2) as

$$\dot{\boldsymbol{\xi}}^R = \mathbf{g}(\mathbf{y},\mathbf{a}^R,\boldsymbol{\xi}^R), \tag{3.3}$$

where $\boldsymbol{\xi}^R(t)=\{\xi_i^R\}_{i=1}^N$ is the adjoint variable. The overall sensitivity of the cost functional $\mathcal{J}$ with respect to $\mathbf{a}^R$ is obtained as

$$\mathcal{S}=\frac{d\mathcal{J}}{d\mathbf{a}^R}=\langle \mathbf{a}^R(t)\boldsymbol{\xi}^R(t)\rangle, \tag{3.4}$$

where $\langle\cdot\rangle$ is any time averaging operator. We can then define the weight matrix Λ with respect to the sensitivity as

$$\Lambda_{ii}=\frac{\mathcal{S}_i}{\max \mathcal{S}_i} \qquad \text{for} \quad i=\{1,\cdots,N\}.$$

In this study we have taken the cost functional $\mathcal{J}$ based on the energy of the temporal modes as

$$\mathcal{J}=\frac{1}{2}\int_0^T \sum_{i=1}^N (a_i^R(t))^2 dt. \tag{3.5}$$

The above functional is minimized subject to the constraint (3.2), by the method of Lagrange multipliers with the adjoint state equation of (3.3) given by

$$\dot{\boldsymbol{\xi}}(t)=-a_i(t)-\sum_{i=1}^N \left(L_{ij}+\sum_{i=1}^N \left(Q_{jik}+Q_{jki}\right) a_k(t) \right) \xi_j(t). \tag{3.6}$$

4 Application of POD ROM for cavity flows

The typical cavity flow configuration used in this study is shown in Fig. 2. The cavity is of an L_e/D ratio of 2. The flow is initialized by a laminar boundary layer so as to have a thickness of $\delta/D=0.28$ at the leading edge of the cavity. The Reynolds number of the flow based on the cavity depth is 1500 and the flow Mach number is 0.6. The equations of Navier-Stokes are discretize using a 4^{th} order accurate scheme in time and space. Snapshots are taken once the flow has stabilized and 56 snapshots are uniformly sampled which corresponds to 1 period of the flow oscillation (2.8 in non dimensional time) corresponding to the first Rossiter mode [29]. Fig. 3 demonstrates a degenerate eigen-spectrum showing eigenvalues which occur in pairs. Also the first 4 eigenmodes capture around 98.5% of the total fluctuation energy as shown by the Relative Information Content (RIC) defined as $RIC(i)=\sum_{j=1}^i \sigma_j/\sum_{j=1}^M \sigma_j$. The temporal coefficients shown in Fig. 4 and demonstrates a phase difference of $\pi/2$ between the paired modes. The representation of the first 4 spatial POD modes for the vorticity is shown in Fig. 5.

Although the modes occur in pairs and their values are distinct the representation is topologically equivalent. We note that the cascade of the energy in the POD representation in terms of the size of the eddies represented. The vorticity being a hydrodynamic phenomenon represents the low frequency dynamics of the flow. In Fig. 6 a comparison of the two weight matrix used for the purpose of calibration is given. We note a similar

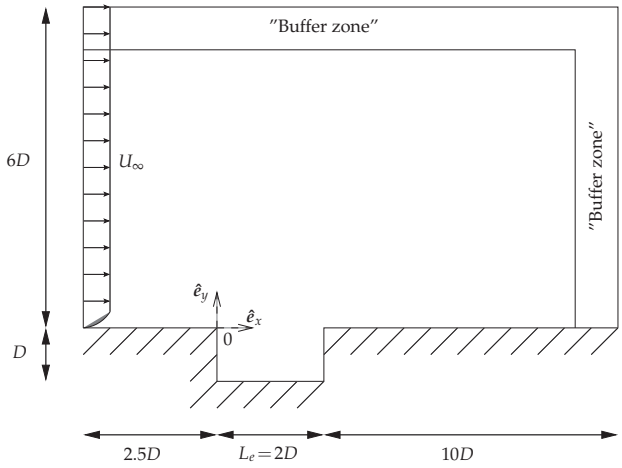

Figure 2: Cavity configuration and computational domain.

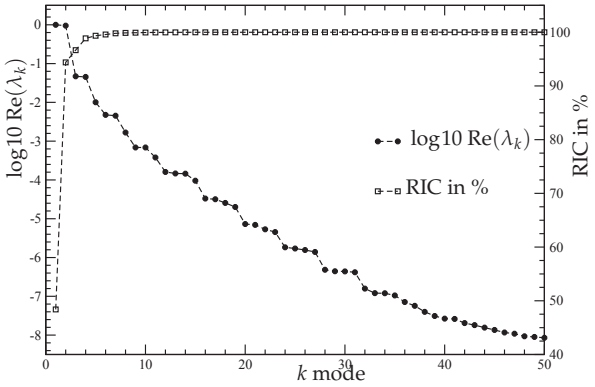

Figure 3: Real part of the eigenvalues and Relative Information Content (RIC).

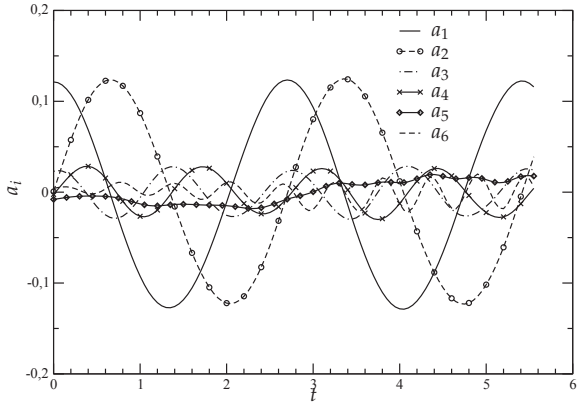

Figure 4: First 6 POD temporal coefficients.

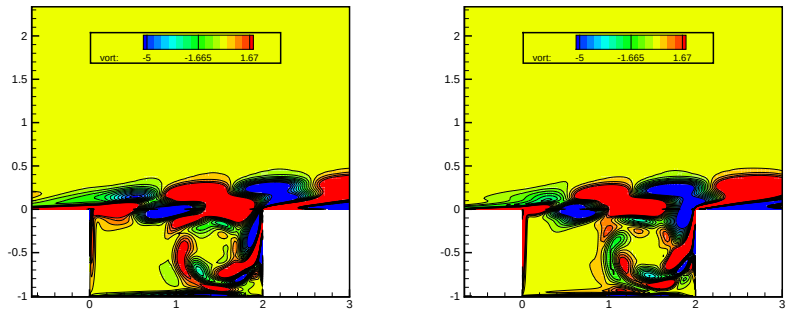

(a) mode 1 (b) mode 2

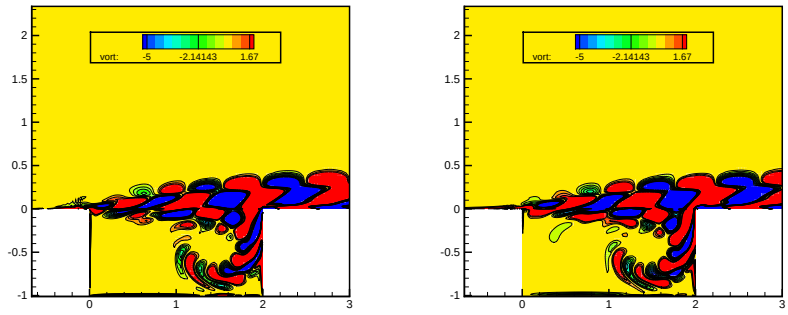

(c) mode 3 (d) mode 4

Figure 5: Vorticity contours of the first 4 POD modes. 15 contours in the range $[-5, 1.67]$ are plotted.

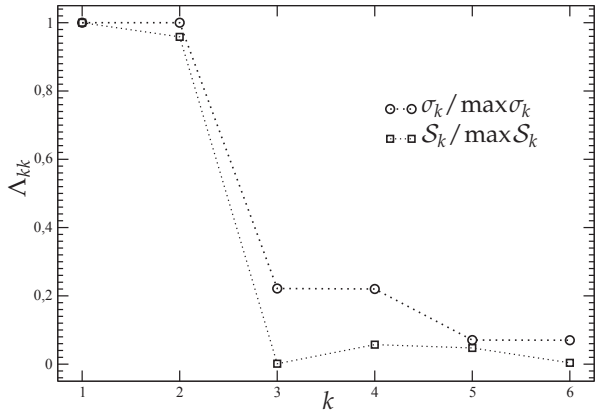

Figure 6: Comparison of the weight matrices used in definition of errors. (a) Weight matrix based on the eigen spectra of the POD, *i.e.* $\frac{\sigma_k}{\max\sigma_k}$; (b) Weight matrix based on the sensitivity analysis for the cost functional based on energy, *i.e.* $\frac{\mathcal{S}_k}{\max\mathcal{S}_k}$.

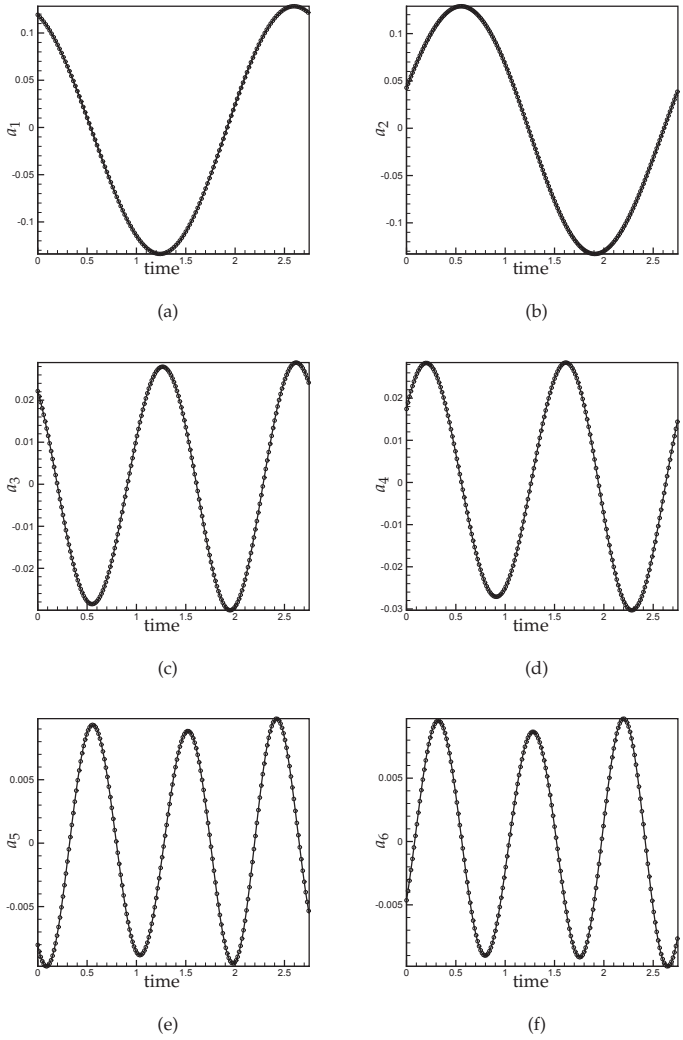

Figure 7: Temporal comparison of the first 6 modes, with the POD coefficients:ROM calibrated (solid line), reference POD dynamics (o). POD ROM is calibrated using the $\mathcal{I}^{(3)}$ minimization for all coefficients. The Tikhonov regularization is applied for ($L=0$, $\mathbf{y_0}=0$), and the weight matrix Λ based on the overall sensitivity.

behavior between the two weights as an energy based cost functional is used in both the cases[†]. The sensitivity based weight is different for mode 3, and this allows us to speculate that in the case where the ROM is not built using the POD bases, but on a different criteria, such as the observability as described in [30], the above analysis may yield a sensitivity weight for the lower modes.

The time evolution and phase plot for the case of the calibrated model is shown in

[†]Although the sense of energy is different in two cases, it is a energy of projection in the case of POD and the energy contained of the flow dynamics, for the sensitivity based analysis.

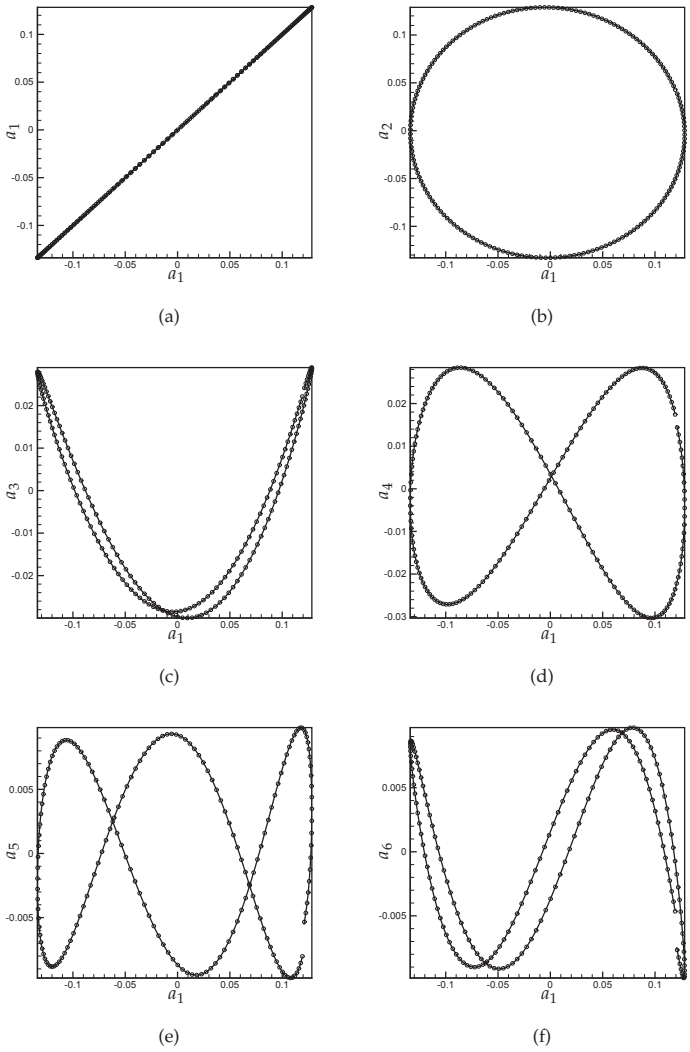

Figure 8: Phase portrait comparison of the first 6 modes, with the POD coefficients:ROM calibrated (solid line), reference POD dynamics (o). POD ROM is calibrated using the $\mathcal{I}^{(3)}$ minimization for all coefficients. The Tikhonov regularization is applied for ($L=0$, $\mathbf{y_0}=0$), and the weight matrix Λ based on the overall sensitivity.

Fig. 7 and Fig. 8 respectively. For the case of the introduction of the actuation mode, snapshots are obtained from the DNS by introducing an actuation of the form $A\sin(\omega t)$ just before the leading edge of the cavity ($x\in[-0.15;-0.05]$ and $y=0$), where the flow is more sensitive to actuation. The spatial modes for the components of velocity are shown in Fig. 9 and exhibit a local behavior capturing the effect of actuation which is the salient feature of the L_2 optimization method. The difference in average values $\delta\boldsymbol{q}^{ac}$ for the stream-wise and span-wise component of velocity u, v is shown in Fig. 10. The value of the error in the projection ε_i as described in Eq. (2.19) is shown in Fig. 11, showing

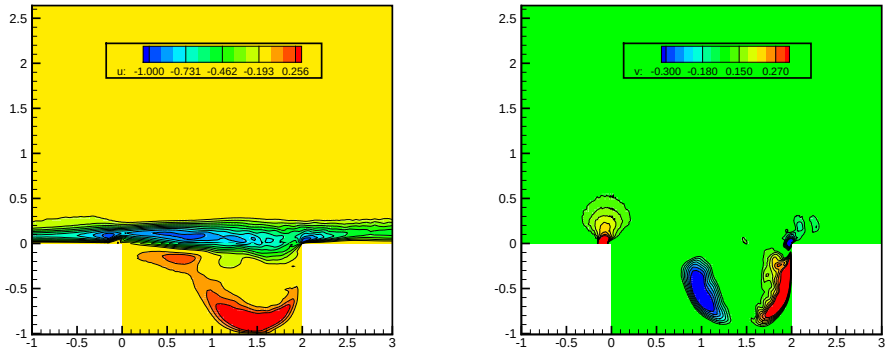

(a) (b)

Figure 9: u and v velocity components of the actuation mode $\boldsymbol{\psi}$ corresponding to an actuation defined by $v_{wall} = 0.2\sin(0.4t)$.

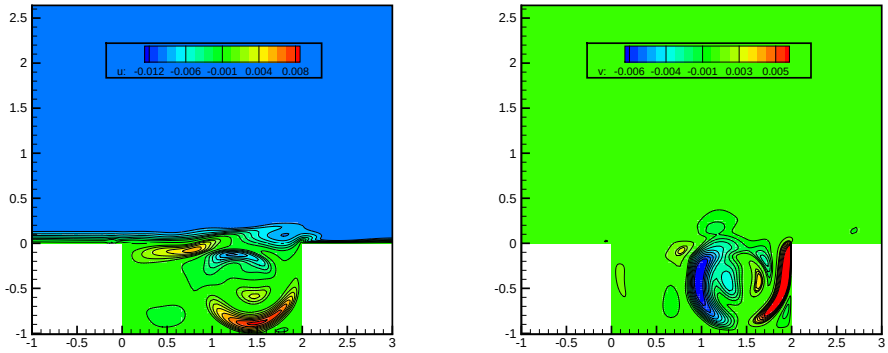

(a) (b)

Figure 10: u and v of the difference in the average value $\delta\overline{\boldsymbol{q}}^{ac}$ between the actuated and the unactuated case.

a small errors for the most energetic modes. We are unable to explain the behavior of the error at the certain higher modes which seem pretty large. Since we are dealing with periodic flow it is natural to expect the temporal dynamics be valid for a time longer than the period of snapshot acquisition. As shown by [31] although the system is initialized with correct state the solution may drift away for a long period of integration even after calibration. Fig. 12 shows that the calibrated model predicts the dynamics for a non-dimensional time 11, which corresponds to around 4 cycle of the flow period, after which it diverges rapidly.

This is different from the results where the calibrated model is shown to work for a much longer period. The reason is that the neglected modes which contribute to the regularization of the system is not modelled during calibration. The validity of ROM for

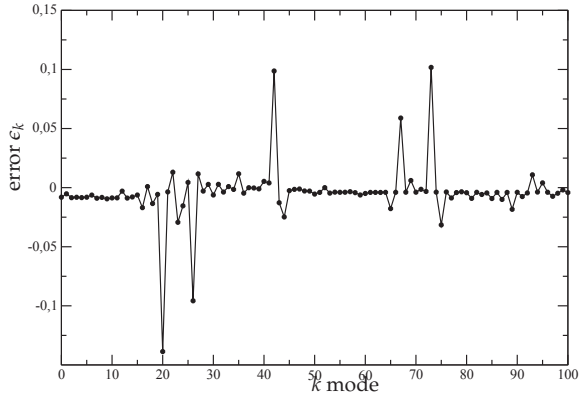

Figure 11: Average projection error ε_k.

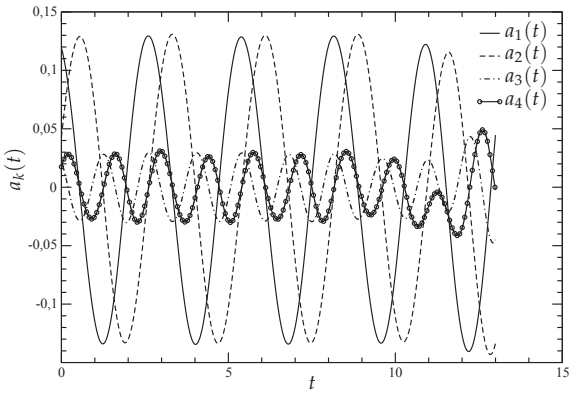

Figure 12: Evolution of first 4 temporal modes of the state of the ROM $a_k(t)$ for a time integration greater than the period of validity of the model. The model diverges after a time $t=11$.

a longer time of integration is still open, where the coefficients need to be given suitable weights to model the neglected term. While performing control, since the time period where the control law is applicable is much larger than the period of validity of the model, it is imperative that we calibrate more than one period of the flow as demonstrated in the next section.

5 Feedback design

In this section we propose a feedback law based on an observer design, obtained from the pressure measurements inside the cavity. The plant model utilized in this study is shown in Fig. 13. It consists of the system *i.e.* linearized ROM and a feedback controller. When all the states of the system are difficult to measure we build an observer to estimate the state while only measuring the output. Regarding the use of ROM for optimal

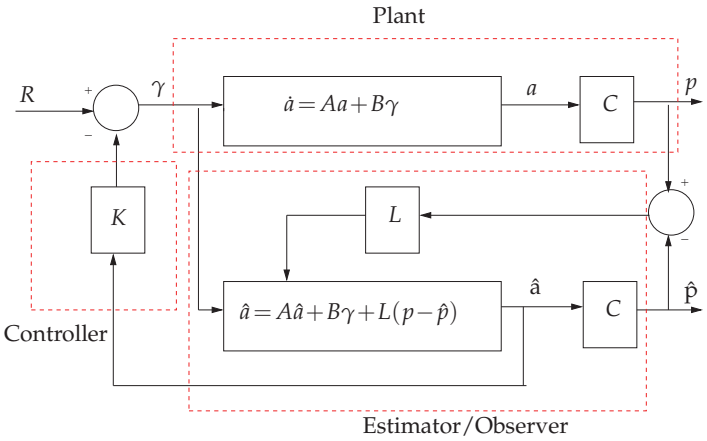

Figure 13: Plant and observer for feedback control. C: observer, L: Estimator, K: Feedback.

control studies one can refer [6,32,33] where the optimal control has been applied for the control of wake flows behind a cylinder. Since the ROM is designed for a particular flow condition, [34] propose a method where the model is refined during the optimization process, to take care of the validity of the model to the variation of control parameters. This method has been applied for the optimal control of wake flows by [35]. Control of cavity flows, using experimental data to build the ROM has been performed in [12], but without any calibration of the temporal dynamics. In this work, the feedback law is determined using the linear part of the dynamical system, neglecting the influence of the quadratic terms. When information of the full state a is not available, an observer $\tilde{C}$ is construct from the measured output y. This is true in case of experimental data, where wall sensors to measure the instantaneous pressure are used. Prediction of flow field from the observed states has been studied in the past by performing a Linear Stochastic Estimation (LSE) by [36,37], where sensor signals are correlated with flow data base information. A higher order correlation is also demonstrated in [38], where a Quadratic Stochastic Estimation (QSE) is performed. The main drawback of the LSE and QSE is that they take into account the correlations at a particular time only without considering the time history of the previous measurements, hence they are termed as 'static' estimators. In an experimental setup this poses a problem due to the measurement noise and also on the limitations of the number of sensors that can be placed. A combination of the isentropic model with the data obtained from experiments has been studied in [12]. The technique of LSE which is used in this work for observer design is briefly explained in the next section.

5.1 Linear Stochastic Estimation (LSE)

The LSE technique enables us to determine the observer matrix $\tilde{C}$, as shown in Fig. 13, given a limited number of pressure measurements obtained from sensors along the walls

of the cavity. For each sensor $i \in [1 \;\; N_s]$, we can estimate the pressure $\tilde{p}_i(t)$ coefficients by a series expansion of the discrete temporal POD coefficients $a_j(t)$ as

$$\tilde{p}_i(t) = \sum_{j=1}^{n} \tilde{C}_{ij}\, a_j(t) + \sum_{j=1}^{n}\sum_{k=1}^{n} \tilde{D}_{ijk}\, a_j(t) a_k(t) + \cdots. \tag{5.1}$$

The expansion can be truncated above the linear term or the quadratic term corresponding to the LSE or QSE problem. The coefficients $\tilde{C}_{ij}$ and $\tilde{D}_{ijk}$ are determined so as to minimize the mean square error between the estimated pressure signal $\tilde{p}_i(t)$ and the one obtained from measurement $p_i(t)$

$$e_i = \int_0^T [\tilde{p}_i(t) - p_i(t)]^2 \, dt = \langle [\tilde{p}_i(t) - p_i(t)]^2 \rangle. \tag{5.2}$$

Since the number of snapshots is much larger than pressure sensors, the above system is overdetermined and the coefficients are determined using the method of least squares by solving an overdetermined linear system given by

$$\frac{de_i}{d\tilde{C}_{ij}} = 0 \quad \text{and} \quad \frac{de_i}{d\tilde{D}_{ijk}} = 0. \tag{5.3}$$

On noting the orthogonality of the temporal modes $\langle a_j, a_k \rangle = \sigma_i \delta_{jk}$, the pressure field can be simply expanded in terms of the temporal modes as

$$\tilde{p}_i(t) = \sum_{i}^{N} \tilde{C}_{ij} a_j(t), \qquad \text{where} \qquad \tilde{C}_{ij} = \frac{\langle p_i, a_j \rangle}{\langle a_j, a_j \rangle}. \tag{5.4}$$

In this study $N_s = 4$ sensors along the wall are used to measure the pressure. It is also worthwhile mentioning that solving the system of equation given by (5.3) leads to an ill conditioned problem. A luxury afforded by numerical simulations is that we can modify the condition number by changing the location of the pressure sensors, however for data obtained from experimental simulations where the sensor positions are fixed we can use the method of Tikhonov regularization mentioned in Section 3.2. The observer dynamics for the construction of the pressure signals, issued from (5.4) is shown in Fig. 14, and provides a good estimation of the wall pressure, due to the orthogonality property of the eigenmodes.

5.2 Linearization of the plant

Once through the observer design, the plant (2.18) is built by linearizing the ROM around a suitable equilibrium point a_0. To determine the influence of various terms of the ROM while linearizing, we perform a sensitivity analysis. Sensitivity studies help in analyzing the variation of a given quantity (generally given by a functional) with respect to a parameter of the model. In this study a sensitivity analysis is performed to identify the

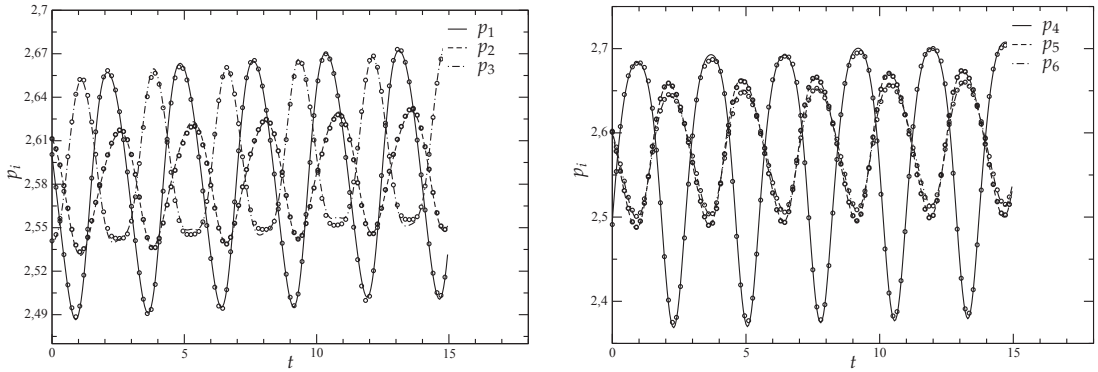

(a) (b)

Figure 14: LSE reconstruction of the pressure signals. The pressure value from the sensor are denoted by line, and the coefficients obtained from LSE denoted by ∘ (one over 3 ∘ are plotted). The sensors are located at positions $(0,D/4)$, $(0,3D/4)$, $(L,D/4)$, $(L,3D/4)$, $(D/2,0)$, $(3D/4,0)$ along the cavity walls and in the shear layer. Unactuated case.

terms to be neglected in the linearization of the model. We seek the sensitivity of the time-independent coefficients h_{1i}, h_{2ij} and h_{3i} of the actuated model, with respect to an energy based functional given by (3.5). A variation of the augmented Lagrangian functional based on an adjoint vector ξ and the state equation (2.18) yield the sensitivities:

$$\frac{\partial \mathcal{J}}{\partial h_{1i}} = \langle \xi_i(t), \gamma(t) \rangle, \qquad \frac{\partial \mathcal{J}}{\partial h_{2ij}} = \langle a_j(t), \xi_i(t)\gamma(t) \rangle, \qquad \frac{\partial \mathcal{J}}{\partial h_{3i}} = \langle \xi_i(t), \gamma^2(t) \rangle, \tag{5.5}$$

and

$$\frac{\partial \mathcal{J}}{\partial \gamma} = \sum_i^n h_{1i}\xi_i(t) + \sum_i^n \sum_j^n h_{2ij}\xi_i(t)a_j(t) + 2\sum_i^n h_{3i}\xi_i(t)\gamma(t),$$

where the adjoint equation is given by:

$$\dot{\xi}_i(t) = g_i(C_i, \boldsymbol{L_i}, \boldsymbol{Q_i}, \boldsymbol{a}(t), \boldsymbol{\xi}(t)) + \sum_j^n h_{2ji}\xi_j(t)\gamma(t) - a_i(t). \tag{5.6}$$

The sensitivities are plotted in Fig. 15 and shows that the constant term of the actuated model h_{1i} has a higher sensitivity when compared to the quadratic terms h_{3i} by an order of magnitude and hence plays an important role in linearization.

It is also important to note that the first two modes which drives the actuation dynamics do not contribute significantly to the sensitivity of the terms h_{1i} and h_{3i} as compared to h_{2ij}, this signifies that more care has to be taken while linearizing these terms.

To determine the equilibrium point a_0 to be used for linearization we solve a nonlinear algebraic matrix equation for the unactuated case $\gamma = 0$. Eq. (2.18) can be recasted for the

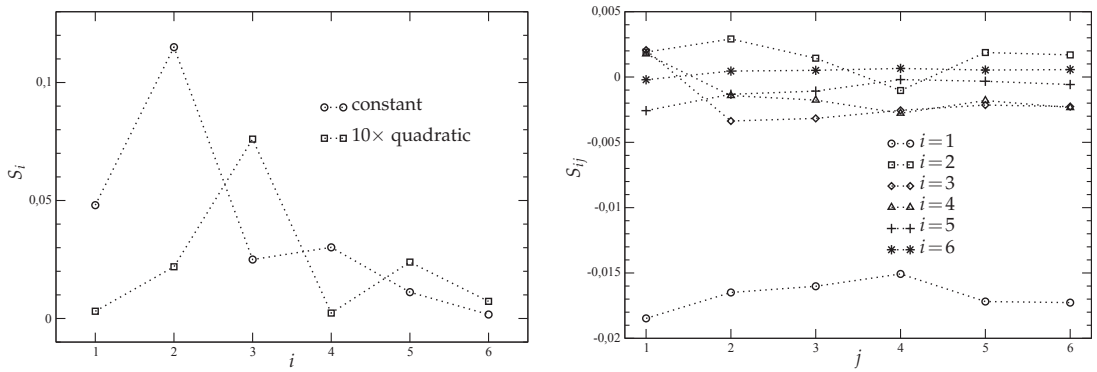

(a) (b)

Figure 15: Sensitivity of the actuated coefficients. Constant: $S_i = \frac{\partial \mathcal{J}}{\partial h_{1i}}$; quadratic: $S_i = \frac{\partial \mathcal{J}}{\partial h_{3i}}$ (rescaled by 10); linear: $S_{ij} = \frac{\partial \mathcal{J}}{\partial h_{2ij}}$.

unactuated part as:

$$f(a) := C + L\boldsymbol{a} + \begin{pmatrix} \boldsymbol{a}^T Q^1 \boldsymbol{a} \\ \vdots \\ \boldsymbol{a}^T Q^N \boldsymbol{a} \end{pmatrix}. \tag{5.7}$$

In this study a Newton's iterative method is used to calculate the equilibrium point $\boldsymbol{a}_0$ using the following algorithm:

$$\boldsymbol{a}_{k+1} = \boldsymbol{a}_k - J^{-1}(\boldsymbol{a}_k) f(\boldsymbol{a}_k), \tag{5.8}$$

where $J(\boldsymbol{a})$ is the Jacobian matrix: $J = \frac{\partial f(\boldsymbol{a})}{\partial \boldsymbol{a}}$. Also note that the solution of the Newton method (Eq. (5.8)) depends on initial conditions and is not unique. To find the equilibrium point, we have chosen the initial conditions of the dynamical system at $t = 0$. On using a linearization at the origin, the plant model can be written in the form (refer to appendix for details)

$$\dot{\tilde{\boldsymbol{a}}} = \tilde{A}\tilde{\boldsymbol{a}} + \tilde{B}\gamma, \qquad \tilde{\boldsymbol{p}} = \tilde{C}\tilde{\boldsymbol{a}}. \tag{5.9}$$

5.3 Controller

After linearizing the plant, one can perform the feedback control. The full plant, control and estimator model are shown in Fig. 13. The model for the controller is given by the equations for a LQG design as

$$\dot{\boldsymbol{a}} = \tilde{A}\boldsymbol{a} + \tilde{B}\gamma + w_1, \qquad y = \tilde{C}\boldsymbol{a} + w_2. \tag{5.10}$$

where for the sake of clarity we denote $a = \tilde{\boldsymbol{a}}$ and $y = \tilde{p}$. The controller noise w_1 and the measurement noise w_2 are assumed to be uncorrelated, zero mean, white Gaussian processes with modelled spectral densities Q_1 and Q_2. In this work the matrices Q_1 and Q_2

matrices are set to identity. We also introduce the noise perturbation vector $\boldsymbol{w} = [w_1\ w_2]$. The response of the state can be separated into three components, the natural response $\boldsymbol{a}_0(\tilde{A},\boldsymbol{a}(0);t)$ which depends on the eigenvalues of the main plant matrix $\tilde{A}$ and on the initial condition $\boldsymbol{a}(0)$, the response to a given control $\gamma(t)$ denoted by $a_\gamma(\tilde{A},\tilde{B},\gamma;t)$ and the response to the noise w_1 given by $a_w(\tilde{A},w_1;t)$. The solution of the plant model (5.10) can be written as

$$\begin{aligned}\boldsymbol{a}(t) &= e^{\,\tilde{A}t}\boldsymbol{a}(0) + \int_0^t e^{\,\tilde{A}(t-\tau)}\,\tilde{B}\,\gamma(\tau)\,d\tau + \int_0^t e^{\,\tilde{A}(t-\tau)}\,w_1(\tau)\,d\tau \\ &= \boldsymbol{a}_0(\tilde{A},\boldsymbol{a}(0);t) + \boldsymbol{a}_\gamma(\tilde{A},\tilde{B},\gamma;t) + \boldsymbol{a}_w(\tilde{A},w_1;t). \end{aligned} \tag{5.11}$$

Assuming a full information state, the feedback law is given by

$$\gamma = -K_c\ \boldsymbol{a}, \tag{5.12}$$

where the matrix K_c is chosen so as to stabilize the plant and minimize the quadratic cost functional given by:

$$\mathcal{J} = \int_0^T \left(\boldsymbol{a}^T W \boldsymbol{a} + \ell^2\gamma^2\right) dt, \tag{5.13}$$

where W is a weight matrix (here it is identity) and ℓ represents the cost of the control. By a simple variational approach, it can be demonstrated that the gain vector K_c is given by

$$K_c = \frac{1}{\ell^2}\tilde{B}^T X, \tag{5.14}$$

where X is the solution of the steady Riccati equation to get infinite horizon stabilization:

$$\tilde{A}^T X + X\tilde{A} - \frac{1}{\ell^2} X\tilde{B}\tilde{B}^T X + W = 0. \tag{5.15}$$

5.4 Observer

In many cases the state $\boldsymbol{a}$ is known only from a limited number of output measurements y, and must be built from an observation $\hat{y}$ which is an approximation of the real value of the measurement y. Denoting $\hat{\boldsymbol{a}}$ the approximation of the state, the observer equations can be written as:

$$\dot{\hat{\boldsymbol{a}}} = \tilde{A}\hat{\boldsymbol{a}} + \tilde{B}\gamma + K_o(y-\hat{y}), \qquad \hat{y} = \tilde{C}\hat{\boldsymbol{a}}. \tag{5.16}$$

The observer gain matrix K_o is obtained by solving the Ricatti equation for Y and the observer matrix $\tilde{C}$ and is given by

$$\tilde{Y}A^T + \tilde{A}Y - Y\tilde{C}^T\tilde{C}Y + Q_2 = 0. \tag{5.17}$$

As described in [39] the observer problem is dual of the controller problem described in (5.15). The estimation gain K_o is obtained finally as

$$K_o = Y\tilde{C}^T. \tag{5.18}$$

5.5 Stabilization of the full system

The full system for the controller and observer, defined in terms of the state and the estimator error $e_a = a - \hat{a}$, with the state denoted by $x = [\boldsymbol{a},\ e_{\boldsymbol{a}}]$, can be written as:

$$\dot{x} = A_t x + D_t \boldsymbol{w}, \tag{5.19}$$

where

$$A_t = \begin{bmatrix} \tilde{A} - \tilde{B}K_c & \tilde{B}K_c \\ (0)_{dim\tilde{A}} & \tilde{A} - K_o\tilde{C} \end{bmatrix}, \qquad D_t = \begin{bmatrix} I_d & 0 \\ I_d & -K_o \end{bmatrix}.$$

To get the system the feedback is applied on the observer state, $\hat{a}$, as $\gamma = -K_c\hat{a}$. The eigenvalue of the full matrix A_t are the same as the eigenvalue of the matrices $\tilde{A} - \tilde{B}K_c$ and $\tilde{A} - K_o\tilde{C}$, and are chosen stable by the Riccati equations. In the absence of any noise, the state errors goes to zero in the infinite horizon, hence the estimation state $\hat{a}$ goes to the real state a, and in the same way, the observer error $e_y = y - \hat{y} = \tilde{C}e_a$ goes to zero. In presence of Gaussian noise $\boldsymbol{w}$, errors e_a and e_y remains under a given threshold, and are functions of the correlation matrices Q_1 and Q_2 as stated in [40]. Following the notation of (5.11), the solution can written as:

$$x(t) = x_0(A_t, x(0); t) + x_{\boldsymbol{w}}(A_t, D_t\boldsymbol{w}; t),$$

where $||x_0|| \to 0$ when $t \to \infty$.

5.6 Application to cavity flow

The control has been designed for different values of the cost $\ell \in [0.01, 5000]$, and the result was found to be roughly independent of the value of ℓ. Finally the value of $\ell = 1$ was chosen for this study. In Fig. 16 the eigenvalues of the open loop matrix $\tilde{A}$ and the closed loop matrix $\tilde{A} - \tilde{B}K_c$ are represented.

The feedback control clearly mirrors the unstable eigenvalues, with dominant eigenvalues of the closed loop $\lambda_{\max} = -0.038 \pm i2.26$. For values of $\ell > 5000$, it seems numerically difficult to use the Matlab system toolbox for the solution of the Ricatti equation, to find an accurate and stable eigenvalue of $\tilde{A} - \tilde{B}K_c$.

The value of the feedback gain $||K_c|| \approx 950$ seems quite large comparing to some usual experimental or numerical data. When $\ell \to \infty$ the cost of the control goes to zero and the system can not be stabilized. In the same manner the norm of the gain goes to zero, similarly when ℓ is small, the efficiency increases due to the large amplitude of the control. However in practical cases the value of the control that can be fed into the actuator is limited by a range of the input signal as a large gain may damage the actuator [12].

To scale down the large gain and to decrease the amplitude of the control, a new parameter α is introduced such that $\gamma_\alpha(t) = \alpha K_c$ with $\alpha \in [0, 1.1]$. In Fig. 17 the real part of the largest eigenvalue of $\tilde{A} - \alpha\tilde{B}K_c$ is plotted with respect to α. The value of $\alpha = 1$ corresponds to the optimal control, while $\alpha = 0$ corresponds to the uncontrolled case.

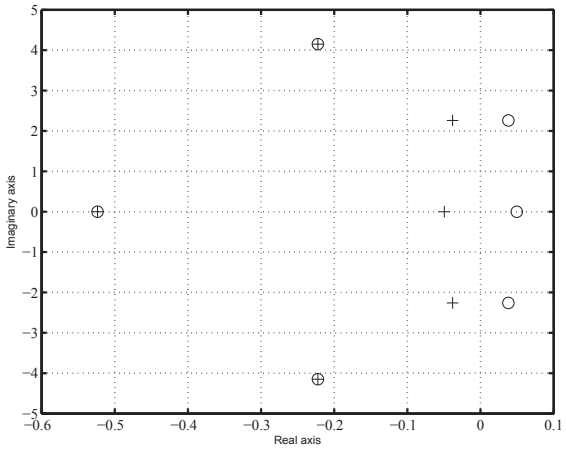

Figure 16: Circle: eigenvalues of the plant; (o): eigenvalues of $\tilde{A}$; ($+$): eigenvalues of $\tilde{A}-\tilde{B}K_c$.

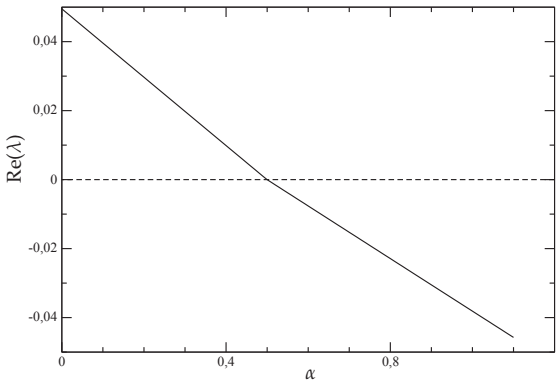

Figure 17: $Re(\lambda_{\max})$ with respect to α.

The value of $\alpha = 0.5$ corresponds to the stability limit of the controlled system, and is the result of mirroring the unstable eigenvalues about the imaginary axis. It means that to stabilize the plant, the norm of the gain control vector should be at least equal to 475, which is a large value for physical application.

The observer response is directly related to the largest eigenvalue of the matrix $\tilde{A}-K_o\tilde{C}$. For our case we found a real value of -0.45 which is sufficient to ensure the decrease of the estimation errors e_a with time. To determine the optimal control input $\gamma(t)_{opt}$, we solve the full system (Eq. (5.19)) and we use the feedback law $\gamma(t)_{opt} = -K_c(a-e_a)$. To remind of the overall procedure, a simulation without control is performed, and the unactuated ROM model is constructed using a Galerkin projection. The model is further calibrated as explained in Section 3.2 to avoid the divergence of solution when integrated in time. To introduce the effect of actuation, the high fidelity model is forced with a chirp

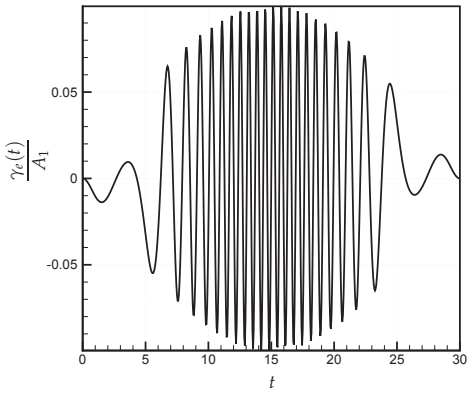

Figure 18: Chirp excitation γ_e: forcing the DNS.

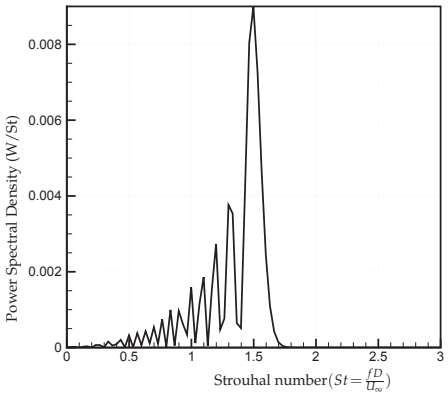

Figure 19: Spectra of the initial chirp.

excitation of the form

$$\gamma_g(t) = A_1 \sin(2\pi St_1 t) \times \sin(2\pi St_2 t - A_2 \sin(2\pi St_3 t)) \tag{5.20}$$

at the upstream corner of the cavity where $A_1 = 0.1$, $A_2 = 27$, $f_1 = 1/60$, $f_2 = 2/3$, $f_3 = 1/30$. The form of the excitation is shown in Fig. 18.

The spectra of the chirp is represented Fig. 19 depicts a large spectral band in the range $0.2 - 1.5$ with a concentration around the value of 1.5.

300 snapshots are sampled in the time interval $t \in [0, T]$ with $T = 15$, corresponding to half the period of excitation of the full chirp. The actuated mode and the plant model are constructed with the help of these realizations. The plant model with the input $\gamma_g(t)$ is simulated. The feedback law $\gamma(t) = -K_c a_g$ is built from the response of the plant $a_g(t)$:

$$\gamma(t) = -K_c \left(e^{\tilde{A}t} a(0) + \int_0^t e^{\tilde{A}(t-\tau)} B \, \gamma_g(\tau) \, d\tau \right). \tag{5.21}$$

The new updated control is found to be of large magnitude max $\gamma(t) = G_{\max} \approx 250$. The evolution of the final optimal control in comparison with the initial solution is as shown in Fig. 20.

A curve fitting approach demonstrates that $\gamma(t)$ is given by

$$\gamma(t) = G_{\max} \sin(\omega t + \varphi), \tag{5.22}$$

where $\omega = 2.27$, corresponding to a non-dimensional frequency $f = 0.3617$ and a phase $\varphi = -1.406$. The frequency is in good approximation to the imaginary part of the largest eigenvalue of the controlled plant (matrix $\tilde{A} - \tilde{B}K_c$). As is seen from (5.21), the gain vector K_c acts as a filter and signals out the frequency which correspond to the shear layer instability of the second Rossiter mode.

To avoid numerical divergence of the numerical solution of the Navier-Stokes equations with the introduction of control, the amplitude (gain) G_0 of any control is set to a

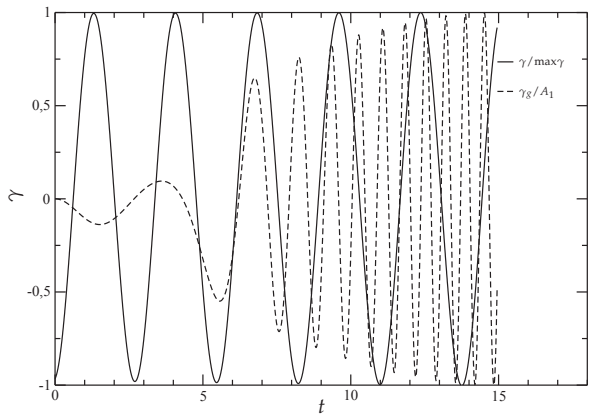

Figure 20: Comparison of the initial forcing $\gamma_g(t)$ and of the final control law $\gamma(t)$.

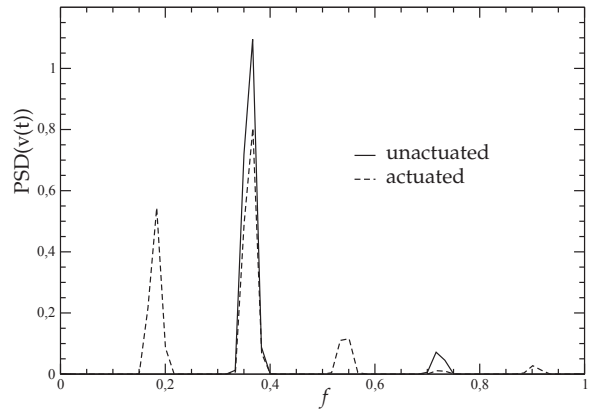

Figure 21: Comparison of Power Spectral Density (PSD) of the original solution and the optimal solution of the normal component of velocity sampled at $y=0$ and $x=1.8D$: Actuated (dashed line); Unactuated (continuous line).

maximum value of $G_0=0.08$. So the updated of control is of the same form as $\gamma(t)$ but with an amplitude G_0. The power spectral density for the vertical component of velocity at a point in the shear layer is compared with the simulation from the unactuated case as shown in Fig. 21 and shows a decrease in amplitude of the second Rossiter mode.

However there is an increase in amplitude at lower frequency due to the effect of actuation as we add energy to the flow. The additional energy goes in furthering the impingement length of the shear layer on the downstream cavity edge, thereby reducing the strength of the pressure signals propagating upstream. The increase in the lower frequency does not correspond to any acoustic modes. The full system response corresponding to (5.19) is shown in Fig. 22 showing an asymptotic stability.

The errors are plotted in Fig. 23, also the response of the observer model is shown in Fig. 24.

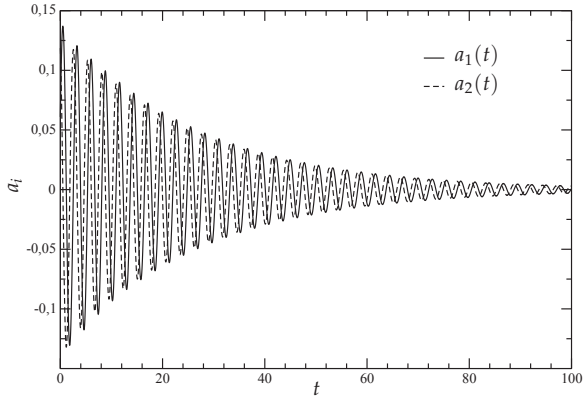

Figure 22: System response of the full system for the state components a_1 and a_2.

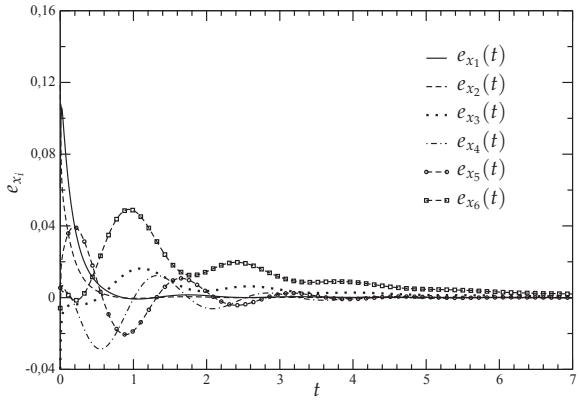

Figure 23: Error on the components of the state e_x.

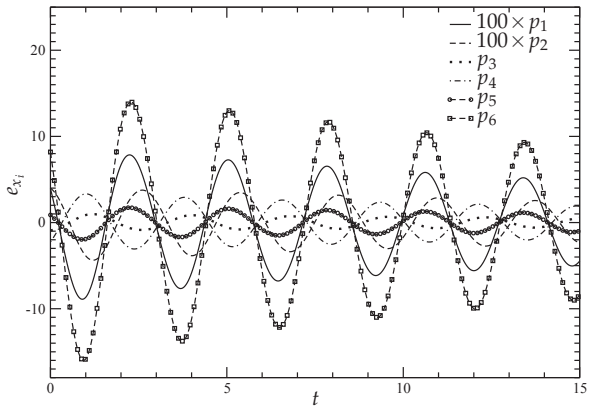

Figure 24: Output prediction y, the pressure fluctuations for the 6 modes. Mode 1 and 2 have been rescaled by 100.

The response of the observer shows that the state for the pressure goes to zero asymptotically, but we find large values of gain for the short period of the DNS simulation, where we implement the control, which necissates the scaling of the final control introduced.

6 Conclusion

In this work different tools of reduced order modelling for the simulation and control fluid systems with instabilities has been presented with an application to cavity flow. The methods presented in this work for the case of a cavity are as well applicable to other systems with instabilities. Numerical simulations were performed to obtain the variables of the isentropic compressible model, which was used to construct the POD Galerkin based reduced order model. Results for the cavity flow configuration has been presented. The extension of the ROM to the actuated case is obtained by solving an optimal problem for capturing the dynamics not captured by the unactuated modes. A new error to measure the effect of actuation on the mean flow has been proposed.

Calibration of the ROM is performed using a Tikhonov based regularization obtained from a sensitivity analysis to obtain an accurate representation of the dynamics. It is also shown that the model diverges for a long time of integration even after calibration, and it is necessary to calibrate over a long period of time, especially when performing control studies.

A feedback control law based on the estimation of the observer dynamics has been presented. The observer matrix is constructed using a linear stochastic estimation. A sensitivity study of the actuated dynamics has been performed to determine the relevant terms in the linearization of the model. Finally an LQG based feedback law is obtained to find the optimal solution. The optimal control law is shown to have a single frequency, corresponding to the second Rossiter mode of the cavity flow. The LQG control provides stabilization over infinite time horizon with a huge control amplitude, unrealistic to be utilized in the Direct Numerical Simulation which are solved over a short time interval. To resolve this problem, the control amplitude has been scaled down before introducing in Direct Numerical Simulation. The control provides a decrease in spectra corresponding to the second Rossiter mode.

As a future perspective it is observed that the POD modes which is an optimal representation of the energy fields is not suitable to resolve the far field acoustic, one of the extension of POD to include the effect of far field acoustic noise is the Most Observable Decomposition, as demonstrated in [30] which represent a good choice of bases to perform control studies for acoustics.

Acknowledgments

This research project has been supported by a Marie Curie Early Stage Research Training Fellowship of the European Community's Sixth Framework Programme under contract

number MEST CT 2005 020301 [41]. We would also like to thank CALMIP center in Toulouse for providing the computational resources. This article has been written in memory of Professor Pierre Comte from PPrime lab, Poitiers, who has made available his DNS code and who tragically passed away in September 2011.

Appendix

To obtain the linearization equation (2.18) can be written as

$$f(a) := C + L\boldsymbol{a} + \begin{pmatrix} \boldsymbol{a}^T Q^1 \boldsymbol{a} \\ \vdots \\ \boldsymbol{a}^T Q^N \boldsymbol{a} \end{pmatrix} + h_1\gamma + \begin{pmatrix} (h^1_{21j}\gamma)^T \boldsymbol{a} \\ \vdots \\ (h^N_{2Nj}\gamma)^T \boldsymbol{a} \end{pmatrix}. \tag{A.1}$$

In this system the quadratic term γ^2 is neglected. As the equilibrium point is unaltered in the presence of a feedback, we introduce a perturbation $\tilde{\boldsymbol{a}} = \boldsymbol{a} - \boldsymbol{a}_0$ to write the above system with the perturbation and the equilibrium state:

$$\begin{aligned} \dot{\tilde{\boldsymbol{a}}} = \dot{\boldsymbol{a}} &= C + L(\tilde{\boldsymbol{a}} + \boldsymbol{a}_0) + \begin{pmatrix} (\tilde{\boldsymbol{a}} + \boldsymbol{a}_0)^T Q^1 (\tilde{\boldsymbol{a}} + \boldsymbol{a}_0) \\ \vdots \\ (\tilde{\boldsymbol{a}} + \boldsymbol{a}_0)^T Q^N (\tilde{\boldsymbol{a}} + \boldsymbol{a}_0) \end{pmatrix} + h_1\gamma + \begin{pmatrix} (h^1_{21j}\gamma)^T (\tilde{\boldsymbol{a}} + \boldsymbol{a}_0) \\ \vdots \\ (h^N_{2Nj}\gamma)^T (\tilde{\boldsymbol{a}} + \boldsymbol{a}_0) \end{pmatrix} \\ &= C + L\boldsymbol{a}_0 + \begin{pmatrix} \boldsymbol{a}_0^T Q^1 \boldsymbol{a}_0 \\ \vdots \\ \boldsymbol{a}_0^T Q^N \boldsymbol{a}_0 \end{pmatrix} + L\tilde{\boldsymbol{a}} + \begin{pmatrix} \tilde{\boldsymbol{a}}^T Q^1 \boldsymbol{a}_0 + \boldsymbol{a}_0^T Q^1 \tilde{\boldsymbol{a}} \\ \vdots \\ \tilde{\boldsymbol{a}}^T Q^N \boldsymbol{a}_0 + \boldsymbol{a}_0^T Q^N \tilde{\boldsymbol{a}} \end{pmatrix} + \begin{pmatrix} \tilde{\boldsymbol{a}}^T Q^1 \tilde{\boldsymbol{a}} \\ \vdots \\ \tilde{\boldsymbol{a}}^T Q^1 \tilde{\boldsymbol{a}} \end{pmatrix} \\ &\quad + h_1\gamma + \begin{pmatrix} (h^1_{21j}\gamma)^T \boldsymbol{a}_0 \\ \vdots \\ (h^N_{2Nj}\gamma)^T \boldsymbol{a}_0 \end{pmatrix} + \begin{pmatrix} (h^1_{21j}\gamma)^T \tilde{\boldsymbol{a}} \\ \vdots \\ (h^N_{2Nj}\gamma)^T \tilde{\boldsymbol{a}} \end{pmatrix}. \end{aligned} \tag{A.2}$$

Since $\boldsymbol{a}_0$ is the equilibrium point of the unactuated model it satisfies (5.7). The terms in (A.2) can be rearranged as the function of the perturbation of the state $\tilde{\boldsymbol{a}}$ as

$$\dot{\tilde{\boldsymbol{a}}} = \tilde{L}\tilde{\boldsymbol{a}} + \begin{pmatrix} \tilde{\boldsymbol{a}}^T Q^1 \tilde{\boldsymbol{a}} \\ \vdots \\ \tilde{\boldsymbol{a}}^T Q^N \tilde{\boldsymbol{a}} \end{pmatrix} + \tilde{h}_1\gamma + \begin{pmatrix} (h^1_{21j}\gamma)^T \tilde{\boldsymbol{a}} \\ \vdots \\ (h^N_{2Nj}\gamma)^T \tilde{\boldsymbol{a}} \end{pmatrix}, \tag{A.3}$$

where

$$\tilde{L} = L + \begin{pmatrix} \tilde{\boldsymbol{a}}_0^T (Q^1 + Q^1)^T) \\ \vdots \\ \tilde{\boldsymbol{a}}_0^T (Q^N + Q^N)^T) \end{pmatrix}, \qquad \tilde{h}_1 = h_1 + \begin{pmatrix} (h^1_{21j})^T \\ \vdots \\ (h^N_{2Nj})^T \end{pmatrix} \boldsymbol{a}_0.$$

The observer model can be written with a perturbation $\tilde{\boldsymbol{p}} = \boldsymbol{p} - \boldsymbol{p}_0$ as:

$$\tilde{\boldsymbol{p}} = \boldsymbol{p} - \boldsymbol{p}_0 = \tilde{C}\boldsymbol{a} - \tilde{C}\boldsymbol{a}_0 = \tilde{C}\tilde{\boldsymbol{a}}. \tag{A.4}$$

The plant model (5.9) is obtained by taking $\tilde{A} = \tilde{L}$ and $\tilde{B} = \tilde{h}_1$.

References

[1] C. W. Rowley, T. Colonius, A. J. Basu, On self-sustained oscillations in two-dimensional compressible flow over rectangular cavities, J. Fluid Mech. 455 (2002) 315–346.

[2] X. Gloerfelt, C. Bailly, D. Juvé, Direct computation of the noise radiated by a subsonic cavity flow and application of integral methods, J. Sound Vib. 266 (1) (2003) 119–146.

[3] G. A. Bres, T. Colonius, Three-dimensional instabilities in compressible flow over open cavities, J. Fluid Mech. 599 (2008) 309–339.

[4] L. Larcheveque, P. Sagaut, O. Labbe, Large-eddy simulation of a subsonic cavity flow including asymmetric three-dimensional effects, J. Fluid Mech. 577 (2007) 105–126.

[5] C. W. Rowley, D. R. Williams, Dynamics and control of high-reynolds number flow over cavities, Annual Review of Fluid Mechanics 38 (2006) 251–276.

[6] M. Bergmann, L. Cordier, J.-P. Brancher, Optimal rotary control of the cylinder wake using POD Reduced Order Model, Phys. Fluids 17 (9) (2005) 097101:1–21.

[7] D. M. Luchtenburg, B. Guenther, B. R. Noack, R. King, G. Tadmor, A generalized mean-field model of the natural and high-frequency actuated flow around a high-lift configuration, J. Fluid Mech. 623 (2009) 283–316.

[8] C. W. Rowley, T. Colonius, R. M. Murray, Model reduction for compressible flows using POD and Galerkin projection, Physica D. Nonlinear Phenomena 189 (1-2) (2004) 115–129.

[9] X. Gloerfelt, Compressible Proper Orthogonal Decomposition/Galerkin reduced order model of self sustained oscillations in a cavity, Phys. Fluids 20 (2008) 115105.

[10] J. Weller, E. Lombardi, A. Iollo, Robust model identification of actuated vortex wakes, Physica D: Nonlinear Phenomena 238 (2009) 416–427.

[11] C. Kasnakoglu, Reduced order modeling, nonlinear analysis and control methods for flow control problems, Ph.D. thesis, Ohio State University (2007).

[12] M. Samimy, M. Debiasi, E. Caraballo, A. Serrani, X. Yuan, J. Little, J. Myatt, Feedback Control of Subsonic Cavity Flows Using Reduced-order Models, J. Fluid Mech. 579 (2007) 315–346.

[13] B. Galletti, C.-H. Bruneau, L. Zannetti, A. Iollo, Low-order modelling of laminar flow regimes past a confined square cylinder, J. Fluid Mech. 503 (2004) 161–170.

[14] M. Couplet, C. Basdevant, P. Sagaut, Calibrated Reduced-Order POD-Galerkin system for fluid flow modelling, J. Comp. Phys. 207 (2005) 192–220.

[15] L. Perret, E. Collin, J. Delville, Polynomial identification of POD based low-order dynamical system, Journal of Turbulence 7 (2006) 1–15.

[16] V. L. Kalb, A. E. Deane, An intrinsic stabilization scheme for proper orthogonal decomposition based low-dimensional models, Phys. Fluids 19 (2007) 054106.

[17] L. Cordier, B. Abou El Majd, J. Favier, Calibration of POD Reduced-Order models using Tikhonov regularization, Int. J. Numer. Meth. Fluids 63 (2) (2009) 269–296.

[18] S. Gugercin, A. C. Antoulas, A survey of model reduction by balanced truncation and some new results, International Journal of Control 77 (8) (2004) 748–766.

[19] B. Moore, Principal component analysis in linear systems: Controllability, observability, and model reduction, IEEE Transactions on Automatic Control 26 (1981) 17– 32.

[20] C. W. Rowley, Model reduction for fluids using balanced proper orthogonal decomposition, International Journal of Bifurcation and Chaos 15 (3) (2005) 997–1013.

[21] A. Barbagallo, D. Sipp, P. Schmid, Closed-loop control of an open cavity flow using reduced order models, J. Fluid Mech. 641 (2009) 1–50.

[22] L. Sirovich, Turbulence and the dynamics of coherent structures, Quarterly of Applied Mathematics XLV (3) (1987) 561–590.

[23] P. Holmes, J. L. Lumley, G. Berkooz, Turbulence, Coherent Structures, Dynamical Systems and Symmetry, Cambridge University Press, Cambridge, U.K., 1996.
[24] L. Cordier, M. Bergmann, Proper Orthogonal Decomposition: an overview., in: Lecture series 2002-04 on the post-processing of experimental and numerical data., Von Karman Institut for Fluid Dynamics., 2002.
[25] E. Caraballo, C. Kasnakoglu, A. Serrani, M. Samimy, Control input separation methods for reduced-order model-based feedback flow control, AIAA Journal 46 (9) (2008) 2306–2322.
[26] D. Rempfer, On low-dimensional Galerkin models for fluid flow, Theor. Comput. Fluid Dyn. 14 (2000) 75–88.
[27] B. R. Noack, P. Papas, P. A. Monkewitz, The need for a pressure-term representation in empirical Galerkin models of incompressible shear flows, J. Fluid Mech. 523 (2005) 339–365.
[28] A. Iollo, S. Lanteri, J. A. Desideri, Stability properties of POD-Galerkin approximations for the compressible Navier-Stokes equations, Tech. Rep. 3589, INRIA (1998).
[29] N. Delprat, Rossiter's formula: A simple spectral model for a complex amplitude modulation process?, Phys. Fluids 18 (2006) 071703.
[30] P. Jordan, C. Tinney, O. Stalnov, M. Schlegel, B. R. Noack, Identifying noisy and quiet modes in a jet, in: AIAA Paper 2007-3702, 2007.
[31] S. Sirisup, G. E. Karniadakis, A spectral viscosity method for correcting the long-term behavior of POD model, J. Comp. Phys. 194 (2004) 92–116.
[32] W. R. Graham, J. Peraire, K. T. Tang, Optimal Control of Vortex Shedding Using Low Order Models. Part 1. Open-Loop Model Development, Int. J. for Numer. Meth. in Engrg. 44 (7) (1999) 945–972.
[33] W. R. Graham, J. Peraire, K. T. Tang, Optimal Control of Vortex Shedding Using Low Order Models. Part 2: Model-based control, Int. J. for Numer. Meth. in Engrg. 44 (7) (1999) 973–990.
[34] M. Fahl, Trust-region methods for flow control based on Reduced Order Modeling, Ph.D. thesis, Trier University (2000).
[35] M. Bergmann, L. Cordier, Optimal control of the cylinder wake in the laminar regime by Trust-Region methods and POD Reduced Order Models, J. Comp. Phys. 227 (2008) 7813–7840.
[36] R. J. Adrian, P. Moin, Stochastic estimation of organized turbulent structure: homogeneous shear flow, J. Fluid Mech. 190 (1988) 531 – 559.
[37] J.-P. Bonnet, D. Cole, J. Delville, M. Glauser, L. Ukeiley, Stochastic estimation and proper orthogonal decomposition: Complementary techniques for identifying structures, Exp. Fluids 17 (1994) 307–314.
[38] M. Buffoni, S. Camarri, E. Iollo, E. Lombardi, S. M. V., A non-linear observer for unsteady three-dimensional flows, J. Comp. Phys. 227 (4) (2008) 2626–2643.
[39] T. R. Bewley, S. Liu, Optimal and robust control and estimation of linear paths to transition, J. Fluid Mech. 365 (1998) 305–349.
[40] S. Bagheri, J. Hoepffner, P. J. Schmid, D. S. Henningson, Input-output analysis and control design applied to a linear model of spatially developing flows, App. Mech. Rev. 62 (2009) 1–27.
[41] K. K. Nagarajan, Analysis and control of self-sustained instabilities in a cavity using reduced order modelling, Ph.D. thesis, Institut National Polytechnique de Toulouse (2010).